PRODUCTION OF THE ALPHA-PARTICLE EMITTING RADIONUCLIDE ASTATINE-211 AT THE TEXAS A&M CYCLOTRON INSTITUTE

A Thesis

by

VIHARKUMAR SATISH BHAKTA

Submitted to the Office of Graduate Studies of
Texas A&M University
in partial fulfillment of the requirements for the degree of

MASTER OF SCIENCE

August 2011

Major Subject: Health Physics

Production of the Alpha-Particle Emitting Radionuclide Astatine-211 at the Texas A&M Cyclotron Institute

PRODUCTION OF THE ALPHA-PARTICLE EMITTING RADIONUCLIDE ASTATINE-211 AT THE TEXAS A&M CYCLOTRON INSTITUTE

A Thesis

by

VIHARKUMAR SATISH BHAKTA

Submitted to the Office of Graduate Studies of
Texas A&M University
in partial fulfillment of the requirements for the degree of

MASTER OF SCIENCE

Approved by:

Co-Chairs of Committee,	Gamal Akabani Hneide
	John Ford
Committee Members,	Robert Tribble
	Craig Marianno
Head of Department,	Raymond Juzaitis

August 2011

Major Subject: Health Physics

ABSTRACT

Production of the Alpha-Particle Emitting Radionuclide Astatine-211 at the Texas A&M Cyclotron Institute.

(August 2011)

Viharkumar Satish Bhakta, B.S., Texas A&M University

Co-Chairs of Advisory Committee: Dr. Gamal Akabani Hneide
Dr. John Ford

The need of a stable production of At-211 is necessary to continue research in alpha-particle targeted radionuclide therapy. Our objectives were to establish the production of Astatine-211 at Texas A&M Cyclotron Institute, optimize the production methods to reduce the generation of contaminants and maximize At-211 production, and assess the radiological safety aspects of At-211 production. The production of the alpha-particle emitting radionuclide At-211 was performed at the Texas A&M Cyclotron Institute using the K500 superconducting cyclotron, following the production reaction Bi-209(α, 2n)At-211 using a thick bismuth target of 500 μm. We carried out two irradiation experiments where the initial energy of the alpha-particle beam, 80 MeV, was degraded using multiple copper and aluminum foils to 27.8 and 25.3 MeV, respectively. The end of beam time was 4 hours for both experiments.

The resulting At-211 yields were 36.0 and 12.4 MBq/μA-h, respectively. Several impurities were produced using the 27.8 MeV, which included At-210 and Po-210. However, when the 25.3 MeV beam was used, the impurities At-210 and Po-210 were

resolved and other contaminants were minimized to less than 0.8% of At-211 yield. The production yields were in accordance with previous published results.

From the success of these initial experiments, additional steps were taken to produce At-211 in excess quantities for distillation purposes. In order to obtain viable quantities of At-211, the gross yield needed to be increased due to losses that are incurred during distillation and radioactive decay. The ability to produce high yields of this isotope required a redesign of the target and use of the K150 cyclotron using a higher beam intensity.

ACKNOWLEDGEMENTS

I would like to thank my committee co-chairs, Dr. Gamal Akabani and Dr. John Ford, and my committee members Dr. Robert Tribble, and Dr. Craig Marianno. Also, I would like to thank Dr. Abeer Alharbi and Dr. Gabriel Tabacaru for their guidance and support throughout the course of this research.

Thanks go to my friends, Akshay Gandhir, Alex Chambers, Mitchelle Carroll, Jessica Hartley, Michael Martin, and Nate Ferdette. I would also like to thank the department faculty and staff for making my time at Texas A&M University a memorable and a great experience.

Finally, thanks to my parents, Satish and Pravina Bhakta, for their encouragement and support through my time at Texas A&M University.

NOMENCLATURE

A	Ampere
Bq	Becquerel
Ci	Curie
EOB	End of Bombardment
FWHM	Full Width Half Max
LET	Linear Energy Transfer
mAb	monoclonal Antibody
NCI	National Cancer Institute
NHL	Non-Hodgkin's Lymphoma
RIT	Radioimmunotherapy
SEER	Surveillance Epidemiology and End Results
SRIM	The Stopping and Range of Ions in Matter
TRT	Targeted Radionuclide Therapy

TABLE OF CONTENTS

Page

LIST OF FIGURES

Page

LIST OF TABLES

Page

1. INTRODUCTION

The Surveillance Epidemiology and End Results (SEER) report published by the National Cancer Institute (NCI) estimated that in 2010 1,529,560 men and women would be diagnosed with cancer in the United States [1]. Of the diagnosed cases, it is estimated that 569, 490 men and women will die from cancer [1]. Currently in the United States, 80% to 90% cancer patients are treated using surgery, chemotherapy and radiation therapy or a combination of these strategies. The remainders of the patients, especially those who have disseminated disease, are treated using palliative methods or experimental biological therapies, such as immunotherapy. However, over the last few decades, there has been a shift in treatment strategies, where physicians and scientists are developing molecular cancer treatments strategies specific to the pathophysiological characteristics of tumors. Among the multiple fields of cancer research, the field of targeted radionuclide therapy (TRT) has received extensive attention.

The initial concept of targeted therapy was first proposed by Dr. Paul Ehrlich in 1898 [2]. Dr. Ehrlich proposed the treatment of disseminated diseases through the use of a concept known as the "Magic Bullet". Dr. Ehrlich coined this term when he described the selective targeting of bacterium without harming the surrounding tissues. This concept of a "Magic Bullet" may be elementary; however, the development of such "Magic Bullet" has been extremely arduous and complex in the area of cancer therapy.

This thesis follows the style of Journal of Nuclear Medicine and Biology.

Due to limitations in knowledge and technology, the concept of targeted therapy remained as a theory until the late 1940s and early 1950s. This theory manifested into a successful experiment by David Pressman, who was able to successfully develop rabbit antibodies that were capable of identifying and targeting tumor malignancies both *in vitro* and *in vivo* experiments [3-7]. Shortly after Pressman's successful attempts, Nungester successfully utilized iodine-131 (I-131) labeled antibodies for the treatment of Wagner osteogenic sarcoma making the first application and use of a radionuclide targeted therapy [8, 9]. These two scientists introduced the concept of targeted radionuclide therapy (TRT). With the successful experiments of Pressman and Nungester, great emphasis was placed on production of radiolabeled antibodies. In 1975, Köhler and Milstein published results of their successful experiments for consistent production methods of monoclonal antibodies (mAbs) [10]. Physicians and scientist could finally conjugate radionuclides with stable mAbs for the treatment of disseminated diseases.

Today, there are two radioimmunotherapy (RIT) drugs approved by the Food and Drug Administration (FDA) for the treatment of cancer, specifically B-cell positive non-Hodgkin's lymphoma (NHL). These are Zevalin (Ibritumomab tiuxetan) and BEXXAR (I-131 labeled tositumomab) approved in 1992 and 1993, respectively [11]. Zevalin and BEXXAR are prescribed to patients with relapsed or refractory low-grade CD20 positive, follicular, or transformed B-cell NHL. The radionuclide utilized in Zevalin is Yttrium-90, a beta emitter whereas iodine-131 is utilized in BEXXAR. Iodine-131 is a mixed beta-gamma emitter. There have been several studies that have compared the

efficacy of these two RIT drugs for the treatment of NHL. A clinical trial at Johns Hopkins University, which involved 38 patients, saw an overall response rate of 50% vs. 44% and complete response rate of 8% vs. 16% for Zevalin and Bexxar respectively [11].

1.1 TRT and Disseminated Diseases

Targeted radionuclide therapy is utilized for the treatment of disseminated diseases due to systemic nature of the diseases involved. TRT strategies are utilized for the treatment of leukemias and lymphomas, metastases from primary cancers, and cancers which have invaded multiple systems within the human body, i.e. lymph nodes. These types of cancer cannot be effectively treated by surgery or radiotherapy due to the invasiveness and inherent risk associated with these treatments. The application of external beam therapy poses unnecessary risks to vital organ systems due to the dose received by normal tissue from treating multiple locations. Therefore, the ability to effectively target the disease and spare normal tissue is compromised. Chemotherapy poses similar risks, as it does not differentiate between normal and tumor tissue. Therefore, the logical strategy is the application of selective, localized radiation using TRT strategies. These strategies can use conjugated mAbs, or other specific targeting agent, with specific radionuclides to effectively treat disseminated diseases.

1.2 Common Radionuclides Used in TRT

In order to create an effective TRT strategy, physical and biological characteristics of the radionuclides must be analyzed. TRT involves the ingestion and injection of particulate radiation with in the human body. Therefore, to minimize residual damage

and dose to normal and healthy organs and tissues, radionuclides which can offer high LET, short range and half-lives are typically considered [12]. There are numerous radionuclides used in targeted radionuclide therapy. These radionuclides have various modes of decay and their radiative emissions can be utilized for the treatment of disseminated diseases [13]. However, radionuclides used for TRT must have certain radiobiological properties. They must be short-lived (short half-life), and decay either via beta (β^-) or alpha-particle (α) emissions [13, 14]. These criteria are required to ensure that the energy of these radiative emissions is deposited locally at the tumor site while minimizing dose to normal tissues. Table 1 provides several common radionuclides currently utilized for TRT.

To maximize delivery of the radioisotope, the physical half-life of the radionuclide must correspond with the biological half-life and overall pharmacokinetics and pharmacodynamics of the mAbs in order to achieve maximum tumor uptake. If the half-life of the radionuclide is longer than that of the mAbs in the tumor volume, then the radionuclide will deposit its energy outside the tumor volume leading to potential normal tissue toxicities, such as hematological toxicity.

Another potential issue is *in vivo* drug stability. After TRT drug delivery, the bond between the mAbs or compound and the radionuclide must remain intact. The radiolabeled compound must be able to withstand changes in radiolysis, blood pH changes, liver catabolism, and *in vivo* blood changes, including immunological reactions. Therefore, a successful TRT strategy must consider both biological and

physical properties of the radiative emission of the radionuclide and the overall pharmacokinetics and pharmacodynamics of the radiolabeled mAb.

Table 1. Physical characteristics of radionuclide utilized for TRT.

Isotope	Half-life (h)	Particle Emitted	Maximum Energy (keV)	LET*	Range in Tissue (mm)
Iodine-131 (I-131)	193	β^-	970	low	2
Rhenium-186 (Re-186)	91	β^-	1,080	low	11
Rhenium-188 (Re-188)	17	β^-	2,120	low	11
Yttrium-90 (Y-90)	64	β^-	2,280	low	1.2
Lutetium-177 (Lu-177)	161	β^-	496	low	1.5
Copper-67 (Cu-67)	62	β^-	577	low	1.8
Bismuth-213 (Bi-213)	0.76	α	8,376	high	0.08
Bismuth-212 (Bi-212)	1	α	8,780	high	0.09
Actinium-225 (Ac-225)	240	α	>6,000	high	0.08
Astatine-211 (At-211)	7.2	α	7,450	high	0.07
Radium-223 (Ra-223)	274.32	α+	>5,000	high	0.08
Thorium-227 (Th-227)	448.32	α+	>6,000	high	0.08

*LET: Linear Energy Transfer. Radiative emissions are divided into low and high linear energy transfer.

1.2.1 Radiobiological Properties of Alpha-Particle Emitting Radionuclides Used in TRT

The enhanced cytotoxicity of alpha-particles makes them extremely attractive for use in TRT [12]. The radiobiological rationale for the use of alpha-particle emitters, such as At-211, is based on the fact that alpha-particles have a very short range in tissue (< 100 μm), making them well matched to cell-specific targeting and highly focal cell killing while sparing normal tissues. Furthermore, because of their high linear energy transfer (LET ~ 100 keV μm^{-1}), they have a greater relative biological effectiveness (RBE), which is about 1,000 times more effective than beta-particles. In contrast to beta-particles, alpha particles are also effective in hypoxic and normoxic tissue conditions, showing a low oxygen enhancement ratio (OER); therefore, they are very effective in eradicating hypoxic radio-resistant tumor cells encountered in most aggressive tumors. This is due to the fact that the biological damage produced by high LET radiations is via direct effects to the cell nucleus. In comparison with low LET radiations, where the majority of the effects are due to indirect effects, and depends on the presence of oxygen to produce free radicals. Finally, the most important radiobiological characteristic of alpha-particles is the absence of dose-rate and cell cycle effects, which makes them extremely compatible with low dose rates encountered in TRT [15]. Figure 1 shows a comparison of the radiobiological characteristics of cell survival fraction between low and high LET radiations.

1.2.2 Preclinical and Clinical Use of Alpha-Particle Emitters

The radionuclide At-211 has been utilized in numerous clinical cancer studies [12, 14, 16-26]. A study at Duke University Medical Center involved the use of At-211

for the treatment of recurrent brain tumors [23, 24]. This study analyzed the production methods of At-211 and labeling of At-211 to mAbs and other biological compounds [12, 23, 25, 26]. The results from open literature showed that the radionuclide At-211 could be produced in therapeutic quantities required for clinical trials (several GBq) and proved the concept of labeling 81C6 anti-tenascin mAb with At-211.

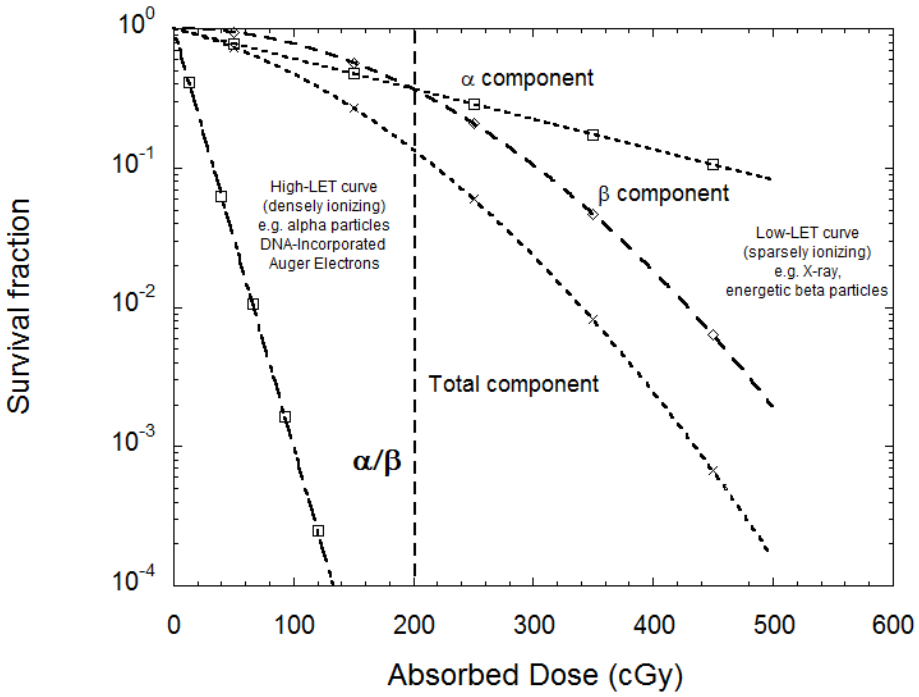

Figure 1. A comparison of the radiobiological characteristics of survival fraction as a function of absorbed dose between low and high LET radiations based on the linear quadratic model.

An *in vitro* study with At-211 observed effects of *in vitro* cytotoxicity of At-211 labeled trastuzumab in several human breast cancer cell lines [16]. This study showed

that the survival fraction of tumor cells when treated with At-211 labeled trastuzumab resulted in a mono-exponential relationship; however, when compared to external beam therapy, the survival fraction showed a linear-quadratic model relationship.

1.3 Purpose

Currently in the United States, there are numerous facilities capable of producing medical radionuclides on a daily basis. However, only three facilities have the capability of producing the radionuclide At-211. These facilities are located at Duke University Medical Center, Durham, NC, the National Institutes of Health, Bethesda, MD, and Washington University, Seattle, WA. In order to further facilitate preclinical and clinical trials that require the use of At-211 for TRT, we studied the feasibility of a viable production method which must be established for proof of concept and to optimize the process. Therefore, the goal of this study was to produce the radionuclide At-211 at the Texas A&M University Cyclotron Institute utilizing the K500 superconducting cyclotron.

2. EXPERIMENTAL METHODS AND MATERIALS

2.1 The Radionuclide Astatine-211

Astatine is a rare element as it is not a naturally occurring element. Therefore, to obtain an isotope of this element, bombardment of other naturally occurring isotopes is required. Particularly for At-211, bombardment of Bi-209 with an alpha-particle yields the production of At-210 and At-211 with threshold energy of 28 and 22 MeV respectively [12, 18, 20-22, 25-34]. In this study, production of At-211 is investigated while searching for methods to minimize production of contaminants.

The radionuclide At-211 is considered a pure alpha-particle emitter due to its decay characteristics (Figure 2). This radionuclide has two specific modes of decay, electron capture and alpha particle emission, with a half-life of 7.241 hours. Table 2 contains the radiative emission for the decay of At-211, where α, ε, and γ denotes alpha-particle, electron capture, and gamma-ray emissions, respectively. The radionuclide At-211 when decaying via alpha-particle, results in the formation of Bi-207. Bi-207 has an extremely long half-life (31.55 years denoted as "a") and it decays via electron capture. The radiative emissions of Bi-207 are provided in Table 3 relative to the decay of At-211. The decay of At-211 via electron-capture results in the formation of Po-211, which is a very short-lived radionuclide (half-life of 0.516 s). The radionuclide Po-211, like At-211, decays via alpha-particle emission and is also considered a pure alpha particle emitter (Table 4). Both Bi-207 and Po-211 decay to a stable isotope of lead (Pb-207). All radiative emissions data were obtained from the LUND/LBNL Nuclear Data [35].

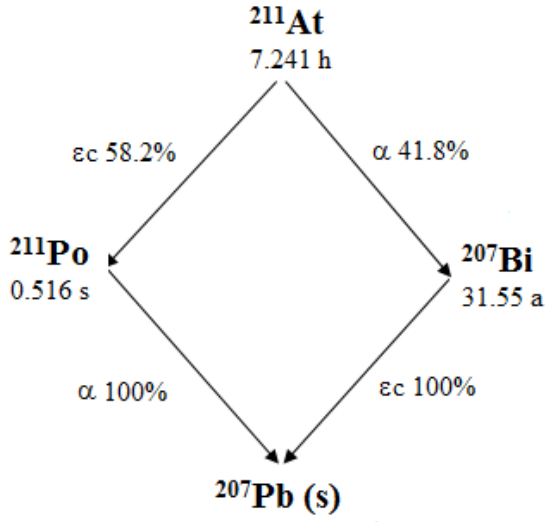

Figure 2. Decay scheme for the radionuclide At-211 [35].

Table 2. Alpha-particle and gamma-ray energies and respective yields for At-211 [35].

Energy (keV)	Rel. Intensity (%)	Decay Mode
5866	41.82	α
99.1	0.274	ε (β^-)
786.1	57.93	ε (β^-)
687	0.261	γ

Table 3. Radiative emissions and yields for Bi-207 [35].

Energy (keV)	Rel. Intensity (%)	Decay Mode
58.25	3.22	ε (β^-)
764.8	38.58	ε (β^-)
569.7	40.87	γ
897.8	0.051	γ
1063.7	31.16	γ
1770.2	2.87	γ

Table 4. Radiative emissions and yields for Po-211 [35].

Energy (keV)	Rel. Intensity (%)	Decay Mode
6570	0.298	α
6893	0.304	α
7450	57.5	α
569.7	0.291	γ
897.8	0.327	γ

2.2 Production of Astatine-211

The production of the radionuclide At-211 has been established via the use of cyclotrons using various targets and reaction channels. The most common reaction channel utilized in the published literature was Bi-209(α,2n)At-211. However, others have tried reactions such as Bi-209(Li-7,5n)Rn-211→At-211, Bi-209(He-3,n)At-211, U_{nat}(p,x)At-211, and Th-234(p,x)Rn-211→At-211 [28]. The most studied method for producing the radionuclide At-211 has remained the Bi-209(α,2n)At-211 reaction due to the availability of alpha-particle beams at the required energy range, the ability to procure Bi-209 targets, and minimal cost involved. This method also allows effective control over the production and minimization of contaminants. Studies using the Bi-209(α,2n)At-211 have been carried out using internal and external target systems [27, 29, 36-38]. Experiments utilizing external and internal targets studied the production of At-211 via direct bombardment of Bi-209 targets or via stacked foils techniques.

The use of internal and external bombardment techniques showed significant variation in production yields of At-211 and contaminants. These discrepancies arise due to the nature of each cyclotron facility, beam profile characteristics, and effective

beam current measurements. Each cyclotron facility has its own inherent characteristics dependent on the equipment utilized, ion source properties, maximum extractable energy, and ability to extract stable beams with high intensity (current) and correct energy. All of these properties can vary from experiment to experiment, thus the variability in results as shown in Table 5.

Table 5. At-211 production yeilds based on previous studies [36].

Source	Eα (MeV)	Target Thickness (μm)	Irradiation Time (h)	Beam Current (μA)	At-211 Yield (MBq/μAh)	Content of At-210
Aaij et al. (1974)	33	500	1 - 2	2 - 4	7.4 - 14.8	0.01 - 0.1%
Rösch el al. (1985)	28	500	5	5	8.56	< 7.10 – 7
Hamwi et al. (1991)	28	30	-	-	27.7	At-210 not detected by γ-spec.
Larsen et al. (1993)	28	250	1-2	10 - 12	8 - 12	At-210 not detected by γ-spec.
Wunderlich et al. (1986)	28	20 (10^{o} offset)	5	5	4	-
Hadley et al. (1991)	28	500 - 800	4	10 - 12	10 - 12	-
Lambrecht and Mirzadeh (1985)	28	100	1.3 - 3.95	6.8 - 9.6	5.3 - 10.4	At-210 not detected by γ-spec.
Larsen et al. (1996)	28	100	0.1396 & 0.1401	7.14 & 1.17	15.2 & 15.6	At-210 activity <0.02% relative to At-211.
	(internal target)	50	1	20 - 40	41 ± 7	

2.2.1 Production at Texas A&M Cyclotron Institute

Production of the radionuclide At-211 was pursued using the K500 superconducting cyclotron at the Texas A&M Cyclotron Institute (Figure 3) [39, 40]. The K500 cyclotron was constructed in 1980s and has gone through several upgrades and improvements since the extraction of the first beam in 1988. This cyclotron is able to produce stable beams ranging from protons, to heavier charged particle beams, such as $(\text{Xenon-129})^{18+}$. Table 6 lists all possible beams that can be extracted from the K500 cyclotron. For the purposes of this study, He^{+} (alpha-particles) beam was extracted for the bombardment of an external target along the MDM beam line.

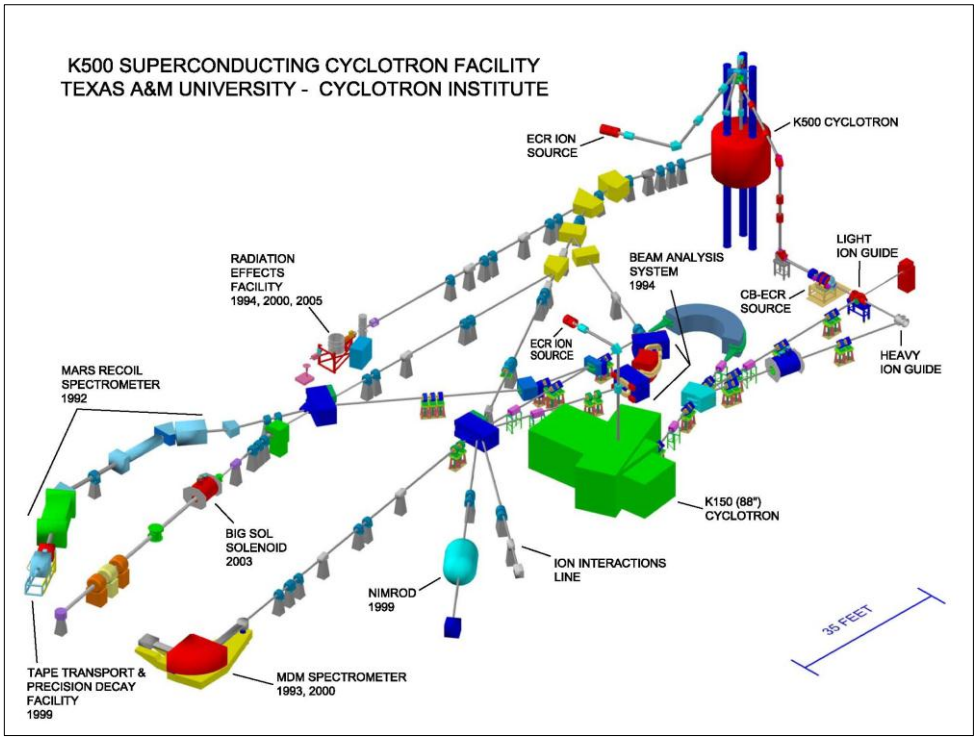

Figure 3. Schematic of K500 superconducting cyclotron facility [40]. The experiments carried out in this research were done at the MDM cave.

Table 6. Beam list for K500 cyclotron as August of 2001 [39, 40].

Ion	E/A (MeV/u)	$I_{extracted}$ (*e*nA)
HD^+	5	70
HD^+	35	15
He-4	15	600
N-14	30.5	120
N-14	40	7
O-16	30	60
Ne-20	14.5	40
Ar-40	2.4	-
Ar-40	20	20
Ar-40	30.5	2
Ar-40	35	1.5
Cu-63	25	3.5
Kr-84	5	1
Kr-84	15	0.3
Xe-129	5	2

HD: Ionized hydrogen

2.3 K500 Cyclotron Beam Analysis

Based on the reaction to be utilized for the production of At-211, the ionized helium beam (He^+) was chosen for bombardment. Energy of the beam was chosen based on preliminary production cross-section analysis obtained from the program TALYS and published literature, including that of the International Atomic Energy Agency (IAEA) [27, 28, 41]. From these preliminary studies, it was determined that the ideal energy for the production of At-211 with a beam of alpha-particles would be 28 MeV. The experiments performed with 28-MeV alpha particles showed that the production of contaminants was minimized while optimizing the production yield of At-211.

2.3.1 Cross-section Analysis

Selection of the alpha-particle beam energy for the first bombardment experiment was primarily based on studies published in the open literature and the IAEA Technical Report Series Number 468. In addition to these studies, the computer code TALYS was utilized to verify the cross-sections for the alpha-neutron reaction [42]. The experimental cross-sections obtained from open literature were obtained through the activation of thin and thick Bi-209 targets [27, 43].

The computer code TALYS simulates nuclear reactions that involve neutrons, photons, protons, deuterons, tritons, helium, and alpha-particles in energy ranges of 1 keV to 200 MeV. This allows the user to theoretically analyze nuclear reactions before experiments are performed. It can also be utilized as a nuclear data tool. Many nuclear reactions have no available data and TALYS can provide data for these reactions via its adjustable parameters. The nuclear reactions considered are those that occur with nuclides with atomic mass of 12 or higher. TALYS utilizes several nuclear interaction models such as the optical model, direction reactions, compound reactions, level densities, pre-equilibrium reactions, multiple emissions, fission, gamma-ray transmission coefficients, and recoil assessment [42]. TALYS produces as output total and partial cross-sections, energy spectrum, angular distributions, double-differential spectra, residual production cross-section, and recoil data.

After reviewing excitation functions and published data for the Bi-209(α,2n)At-211 reaction, the threshold energy was determined to be 22 MeV and optimal bombardment energy range was established between 22 and 28 MeV. However, in this

energy range there are other open reactions, such as Bi-209(α,3n)At-210 and Bi-209(α,t)Po-210 which are considered contaminants (Section 3.1). Direct production cross-section for these three reactions from simulations with TALYS are presented in Figure 4. Table 7 compares cross-section values in the optimal energy range for Bi-209(α,2n)At-211 reaction. After assessing published cross-section data and TALYS output, an alpha-particle with an initial energy of 28 MeV was chosen for the first experiment.

Table 7. Cross-sections for Bi-209(α,2n)At-211 reaction.

	Bi-209(α,2n)At-211 (mb)		
Energy (MeV)	TALYS	Lambercht	Hermanne
22	52.79	68.30	77.75
23	165.92	189.23	191.40
24	310.40	348.80	310.82
25	450.26	478.39	449
26	573.62	587.49	550.59
27	681.80	725.40	665.73
28	773.72	800.89	722.07

Possible contaminants associated with the production of At-211 are At-210 via Bi-209(α,3n)At-210 and Po-210 via Bi-209(α,t)Po-210 reactions. At-210 has similar decay characteristics as At-211 with a half-life of 8.1 hours, but it is not considered a pure alpha-particle emitting radionuclide (Figure 5). At-210 primarily decays via electron capture (99.82 %) thus having a low probability of alpha-particle emission. This decay characteristic is prone to multiple gamma-ray emissions dependent on the

energy of the emitted beta-particle. Table 8 provides energies for the emitted particles and gamma-rays and their relative emission intensity for At-210. The radiative emission of At-210 makes it an unattractive radionuclide for TRT based on the properties discussed previously in Section 1.2.

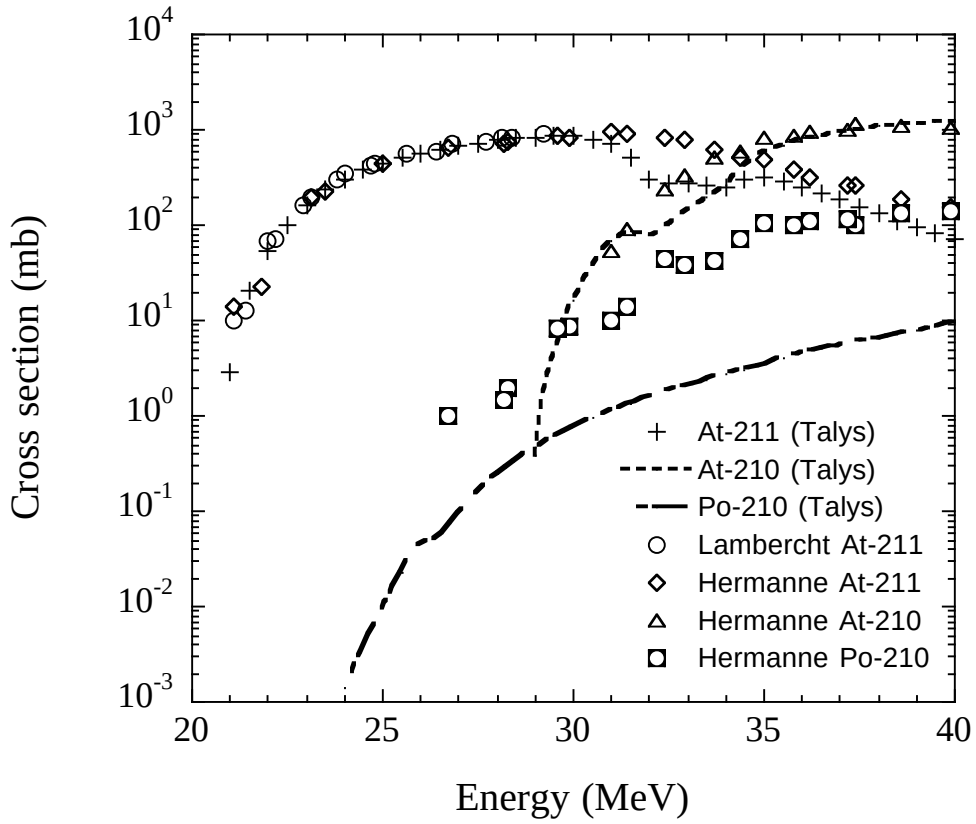

Figure 4. Direct production cross-section for At-211, At-210, and Po-210 [27, 28].

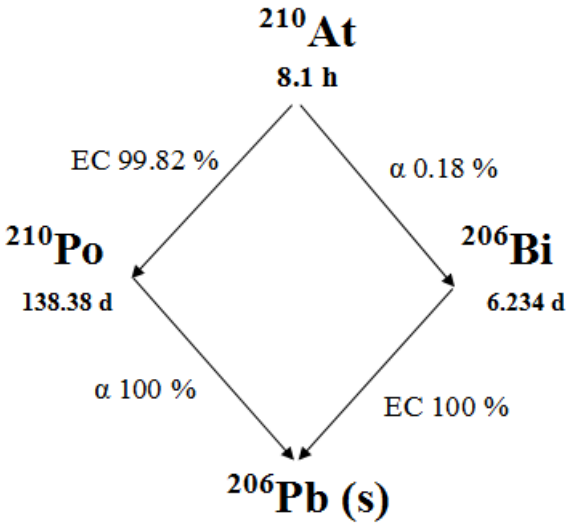

Figure 5. Decay scheme for the radionuclide At-210 [35].

Table 8. Radiative emissions and intensities for At-210 [35].

Decay Mode	Energy (keV)	Intensity (%)
α	5360.9	26.8
	5386	4.6
	5442.4	29.0
	5465	7.8
	5524.1	31.3
ε (β^-)	253.72	5.39
	552.42	2.2
	954.58	19
	1070.95	70
	2507.66	2.9
γ	245.31	79
	1181.39	99.3
	1436.7	29
	1483.39	46.5
	1599.7	13.4

The second potential contaminant is polonium-210 (Po-210). Polonium-210 has a half-life of 138.38 days and the only mode of decay is via alpha-particle emission (5.304 MeV). However, polonium is extremely hazardous to the human body, particularly bone surfaces and liver. If Po-210 is inhaled or ingested, the majority of the activity will be metabolized in the liver and it will be deposited on bone surfaces with biological half-life of 40 and 100 years, respectively. This will result in damage to the liver, bone surfaces and bone marrow posing a serious health risk for the exposed individual. Based on this hazard, great emphasis is placed in minimizing the production of this contaminant.

Along with cross-section data, TALYS also specifies all possible reactions that can occur based on incident particle and target atom. These reactions recoil particles being emitted or other residual radionuclides being produced. For all reactions TALYS computes cross-section, Q-value, and lists all possible particles emitted. This information is extremely useful when performing gamma-ray spectroscopy. Tables 9 – 11 presents the output from TALYS for the Bi-209(α,x) reactions at 28 MeV.

Table 9. Total particle production cross-section for 28 MeV alpha-particles.

Particle Production	Cross-section (mb)
gamma (g)	1.88E+03
neutron (n)	1.56E+03
proton (p)	2.48E-01
deuteron (d)	1.68E-02
triton (t)	2.45E-01
helium-3 (h)	1.91E-08
alpha (a)	2.61E+01

Table 10. Particle production cross-section data for 28 MeV alpha particles.

Reaction	Cross-section (mb)	Emitted Particles					
		n	p	d	t	h	a
(a,g)	6.12E-03	-	-	-	-	-	-
(a,n)	1.17E+01	1	-	-	-	-	-
(a,p)	2.18E-01	-	1	-	-	-	-
(a,d)	1.68E-02	-	-	1	-	-	-
(a,t)	2.45E-01	-	-	-	1	-	-
(a,a')	2.50E+01	-	-	-	-	-	1
(a,2n)	7.72E+02	2	-	-	-	-	-
(a,np)	2.84E-02	1	1	-	-	-	-
(a,nd)	6.31E-07	1	-	1	-	-	-
(a,na)	1.14E+00	1	-	-	-	-	1
(a,pa)	1.88E-03	-	1	-	-	-	1
(a,2a)	1.00E-07	-	-	-	-	-	2
(a,2np)	7.94E-06	2	1	-	-	-	-
(a,2na)	3.63E-02	2	-	-	-	-	1
(a,3a)	1.000E-07	-	-	-	-	-	3

Table 11. Radionuclide production cross-sections for a 28 MeV alpha-particles bombarding bismuth-209 target.

Z	A	Nuclide	Total Cross-section (mb)	Isomeric Cross-section (mb)	Isomeric Ratio
85	213	At-213	6.12E-03	6.12E-03	1
85	212	At-212	1.25E+01	1.25E+01	1
84	212	Po-212	2.18E-01	2.18E-01	1
85	211	At-211	7.74E+02	7.74E+02	1
84	211	Po-211	4.52E-02	4.52E-02	1
84	210	Po-210	2.45E-01	2.45E-01	1
83	209	Bi-209	2.50E+01	2.50E+01	1
83	208	Bi-208	1.14E+00	1.14E+00	1
82	208	Pb-208	1.88E-03	1.88E-03	1
83	207	Bi-207	3.63E-02	3.63E-02	1
81	205	Tl-205	1.00E-07	2.36E-08	0

2.3.2 Beam Degradation Analysis

After performing cross-section analysis to determine the initial energy of the alpha-particle beam, extraction methods for the beam were considered. Based on the external target system being utilized for the experiment, there were two options to obtain the appropriate beam for bombardment. The first option would allow for direct bombardment of the Bi-209 by directly extracting a 28 MeV beam. However, there were concerns that the intensity of the beam would be significantly lower compared to the desired level. Due to these concerns, direct bombardment with K500 was abandoned and analysis for a stacked-foil external target system was performed. Reviews of published experiments with stacked foil system showed that At-211 could be produced at high yields while minimizing production of contaminants [29].

Assessment of published experiments led to the decision to utilize the stacked-foil method. To ensure high beam current could be extracted, the beam was extracted with an initial energy of 80 MeV. This initial energy was attenuated through the use of degrading foils comprised of copper and aluminum foils. The foils and their thickness were chosen such that alpha-particles interacting with the bismuth target would have an average energy of 28 MeV. Beam degradation calculations were performed utilizing the software The Stopping and Range of Ions in Matter (SRIM) and LISE++ [44, 45]. Degradation simulations of the alpha-particle beam were initially performed using the physical calculator of the computer code LISE++, by building a stacked foil system along the MARS-MDM beam line of the K500 cyclotron. These calculations were corroborated using Monte Carlo simulation within the computer code SRIM (Table 12 and Table 13). The foils utilized were based on available thickness of the copper and aluminum foils along with machining capabilities available at the Cyclotron Institute. The SRIM software also provided information with respect to lateral straggling of the beam with the use of the stacked foils (Figure 6). Lateral straggling calculations were simulated using a single point of reference for the incident alpha-particle beam. The diameter of the alpha-particle beam was reduced to 8 mm; therefore, lateral straggling significantly impacts the final energy and intensity of alpha-particles reaching the Bi-209 target. The physical properties of the foils are presented in Table 14.

Table 12. Beam degradation calculation to obtain 28 MeV at Bi-209 target.

Foil	Thickness (μm)	E_{in}[a] (MeV)	E_{out}[a] (MeV)	E_{in}[b] (MeV)	E_{out}[b] (MeV)	σ_{Eout}[b] (MeV)
Cu	100	80.000	74.064	80.000	74.071	0.171
Cu	100	74.064	67.746	74.071	67.744	0.376
Cu	100	67.746	60.957	67.744	60.949	0.326
Cu	100	60.957	53.555	60.949	53.515	0.419
Cu	100	53.555	45.307	53.515	45.245	0.483
Cu	100	45.307	35.773	45.245	35.658	0.630
Al	127	35.773	30.441	35.658	30.213	0.669
Al	50	30.441	28.130	30.213	27.819	0.767
Bi-209	500	28.130	0.000	27.819	0.000	-

*a – LISE++, b - TRIM

Table 13. Beam degradation calculation to obtain 25 MeV at Bi-209 target.

Foil	Thickness (μm)	E_{in}[a] (MeV)	E_{out}[a] (MeV)	E_{in}[b] (MeV)	E_{out}[b] (MeV)	σ_{Eout}[b] (MeV)
Cu	100	80.000	74.064	80.000	74.071	0.171
Cu	100	74.064	67.746	74.071	67.744	0.376
Cu	100	67.746	60.957	67.744	60.949	0.326
Cu	100	60.957	53.555	60.949	53.515	0.419
Cu	100	53.555	45.307	53.515	45.245	0.483
Cu	100	45.307	35.773	45.245	35.658	0.630
Al	127	35.773	30.441	35.658	30.213	0.669
Al	127	30.441	25.665	30.213	25.311	0.966
Bi-209	500	25.665	-	25.311	-	-

*a – LISE++, b - TRIM

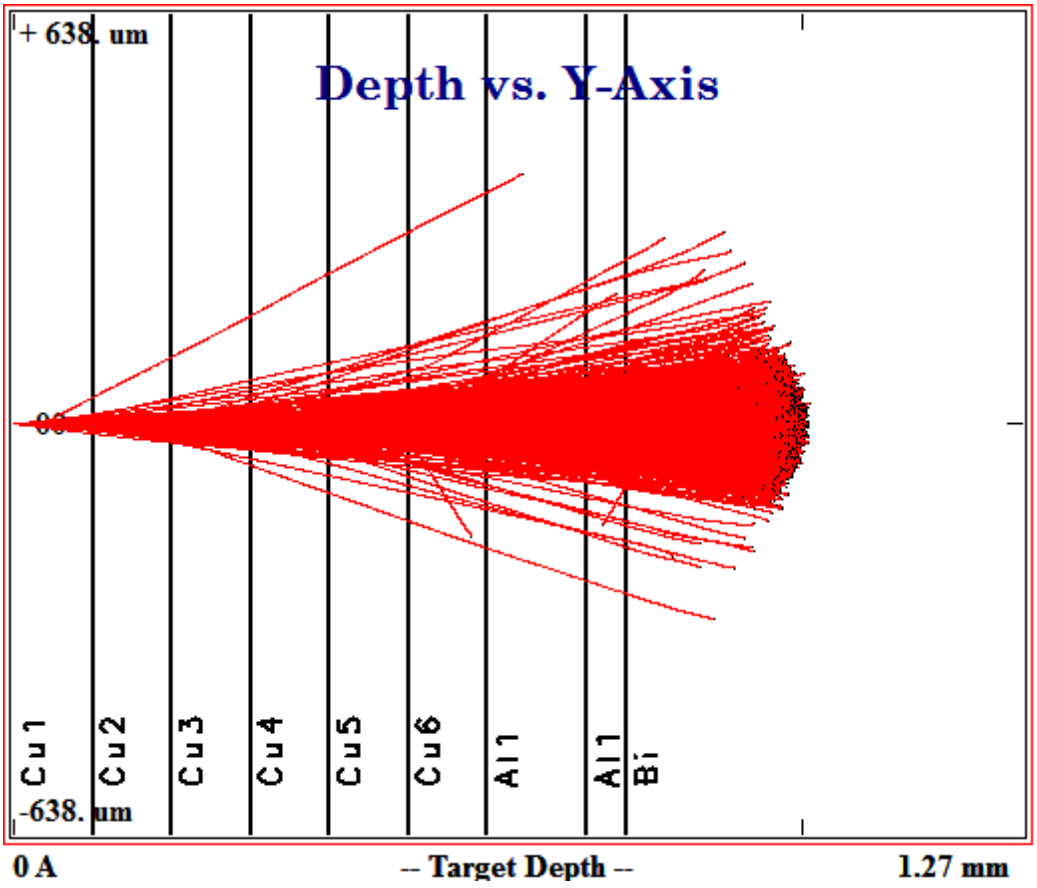

Figure 6. Lateral straggling and range profile for 28 MeV alpha-particles. The characteristics of the foils are given in Table 13. Simulations were performed using a single point of incidence. The diameter of the alpha-particle beam was reduced to 8 mm.

Table 14. Physical properties of stacked foils utilized for At-211 production.

Foil	Density (g/cm3)	Isotope
Copper	8.92	Nat (99.9%)
Aluminum	2.92	Nat
Bismuth	9.81	^{209}Bi (99.999%)

2.4 Target Development

As discussed in Section 2.3.2, a stacked foil external target system was utilized for the production of At-211. We utilized a system that was originally designed by Dr. Abeer Alharbi and Alexandra Aspiridon (personal communication) for other experimental purposes. The foils utilized for the target system had a radius of approximately 1 cm and had varying thickness as required for beam degradation (Table 12 and 13). Figure 7 displays the foil, punch, and ancillary equipment utilized to generate this target system. The initial beam size was reduced to 8 mm in diameter through the use of several collimators as shown in Figure 8. The stacked foils were housed in an aluminum cylinder with insulators on each side. Included in the target cylinder housing was a multimeter to monitor beam current throughout the experiment. Figure 9 displays an enclosed external target system prepared for bombardment. A close-circuit camera system was utilized to monitor the alpha-particle beam before commencement of bombardment.

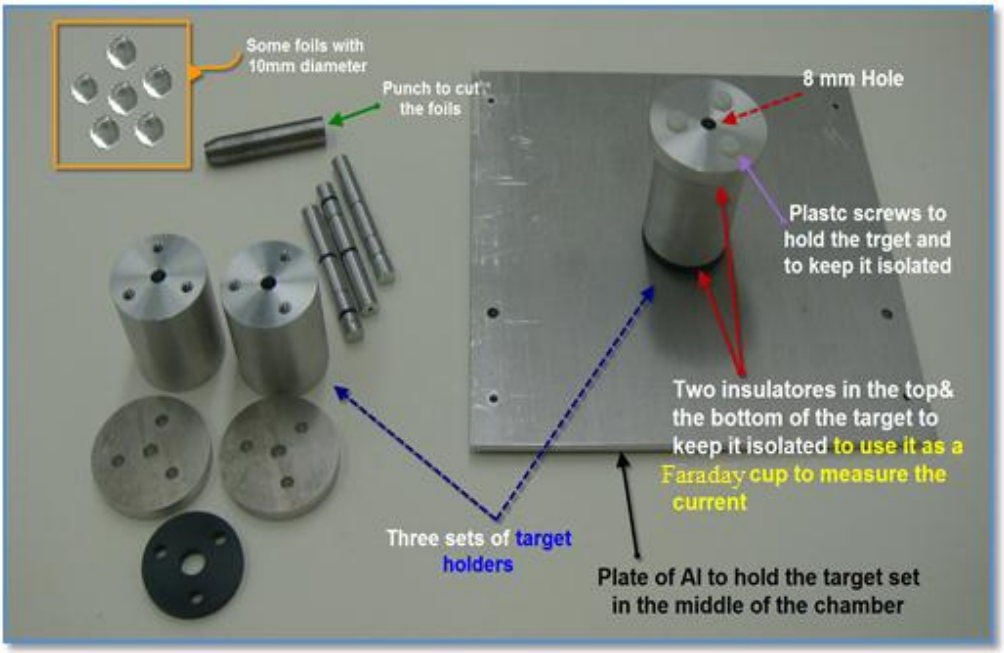

Figure 7. Equipment utilized to build the external target system for At-211 production.

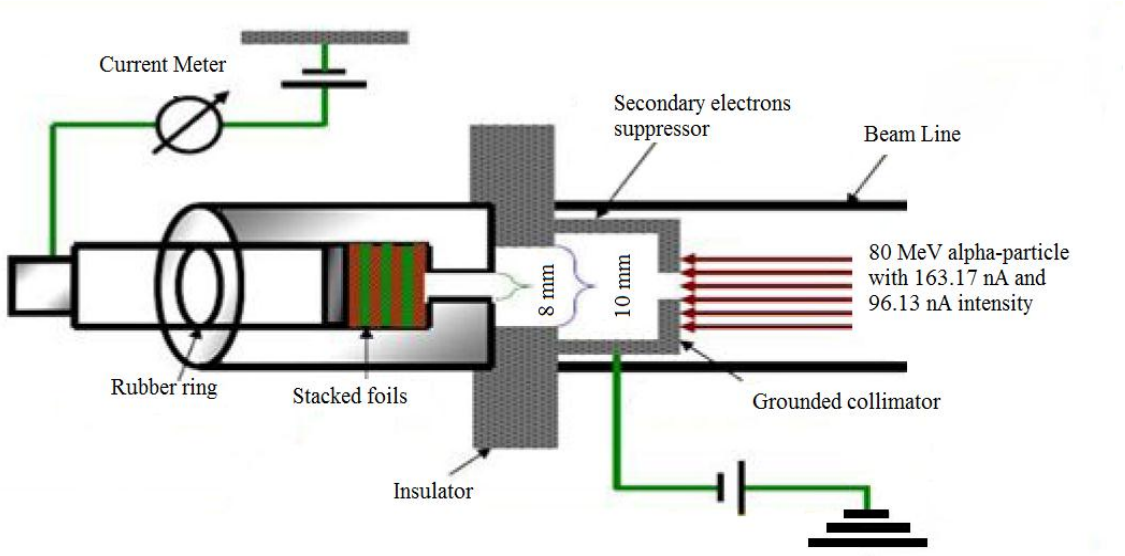

Figure 8. Stacked foil geometry and target holder system for At-211 production.

Figure 9. External target system utilized for the production of At-211. 1) Camera system. 2) Housing of target system. 3) Focusing magnet. 4) Target holder. 5) Faraday cup connections. 6) Vacuum system.

2.5 Detector Calibration

In order to assess the production yields of At-211, a detector counting system was assembled to perform gamma-ray spectroscopy. A Canberra Hyper Pure Germanium (HPGe) detector with an absolute efficiency of 10.9 % was utilized for this purposes. This detector was equipped with a sliding rail system positioned in front of the HPGe detector crystal. The rail system allowed for the movement of an irradiated target and calibration sources to specific distances from the detector. These positions were utilized to characterize the detector efficiency as a function of source distance. Increased distance between the source and the detector can compensate for dead-time effects associated with high activity sources, thus improving quality of obtained spectra.

Calibration of the HPGe detector system was performed with several certified sealed sources consisting of Barium-133 (Ba-133), Cesium-137 (Cs-137), Cobalt-60 (Co-60), and Europium-152 (Eu-152) with an initial activity of 1 μCi [27]. Table 15 lists the decay energies for each radionuclide used for calibration purposes along with their radiological properties. The source spectra were acquired and analyzed using Amptek multi-channel analyzer (MCA) and acquisition software provided by an Amptek. Spectra were acquired at distances of 10, 15, 20, 25, 30, 35, and 50 cm to characterize the efficiency of the detector.

Table 15. Radiological and gamma emissions characteristics of calibration sources utilized for energy calibration and efficiency calculations [35].

Source	Half Life (y)	Energy (keV)	Instensity (%)
Cs-137	30.07	661.657	85.1
Co-60	5.27	1173.27	99.9736
		1332.5	99.9856
Ba-133	10.51	80.9971	34.06
		276.398	7.164
		302.853	18.33
		356.017	62.05
		383.851	8.94
Eu-152	13.537	121.782	28.58
		244.698	7.583
		344.279	26.5
		778.904	12.942
		964.079	14.605
		1085.87	10.207
		1112.07	13.644
		1408.01	21.005

An initial spectrum was acquired for the natural background in order to obtain the characteristics of the detector and to observe any contributions from residual contaminants in the counting room (Figure 10). From the spectrum acquired it was observed that there were no significant residual gamma-ray contributions from the geometry and equipment utilized except for the natural background gamma peak of potassium-40 (K-40) at 1.46 MeV. From preliminary studies of potential production reactions, it was determined that there would not be any conflicts with spectra obtained from irradiated targets (Sections 2.2 and 2.3.1) [28].

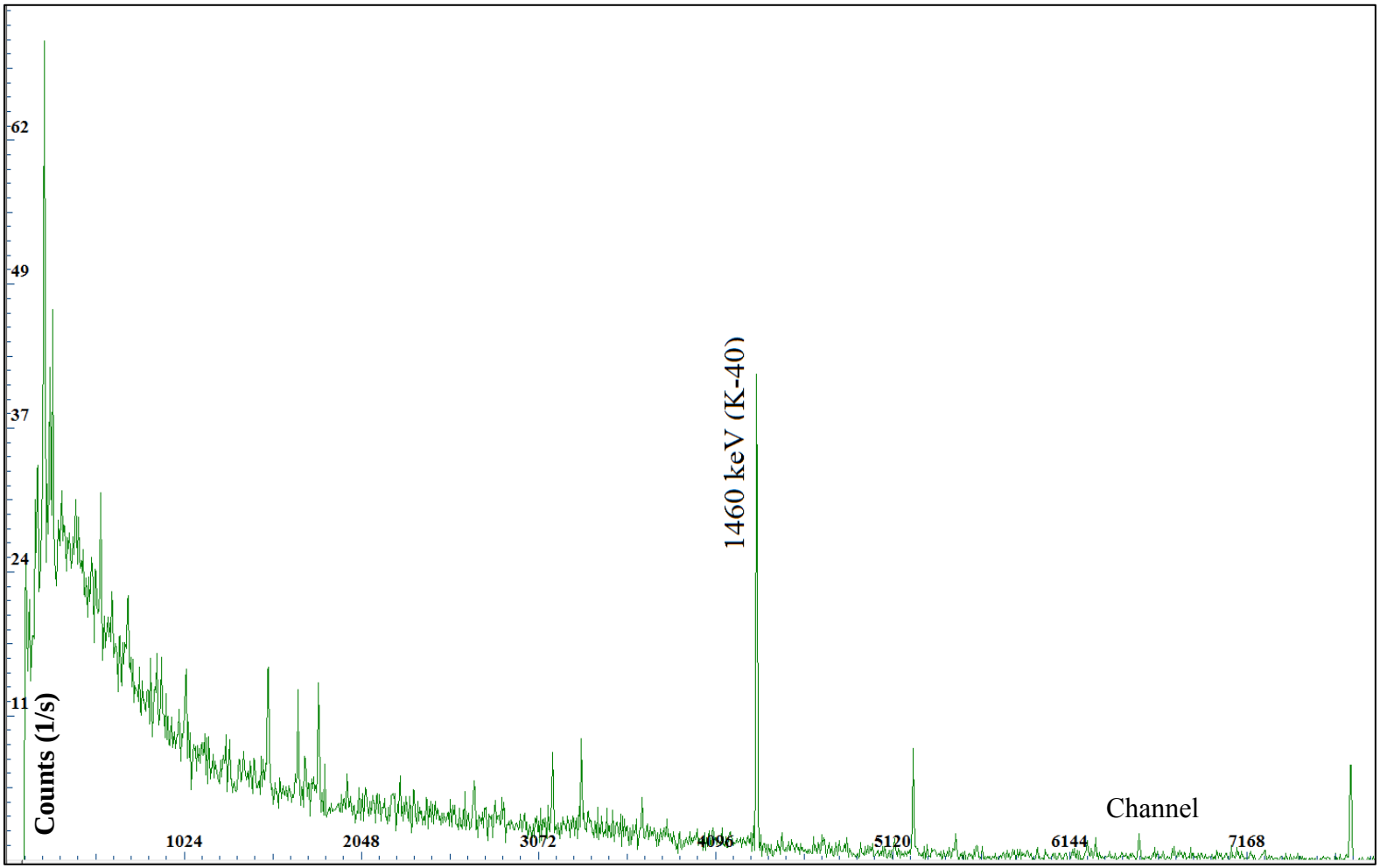

Figure 10. Background spectrum obtained using HPGe detector in the counting room. The only major gamma contribution observed was that of potassium-40 (K-40) at 1.460 MeV.

Initial channel versus energy calibration of the MCA was performed with the Co-60 sources. Co-60 decays via the emission of 1.173 and 1.332 MeV gamma-rays with emission intensity of 99.974 and 99.986 respectively (Figure 11). After loading the spectrum in the ADMCA software, the peaks of Co-60 gamma-rays were associated with appropriate channel numbers. Having two unique energies with corresponding channel, the auto calibration function was able to generate coefficients for the equation utilized to calibrate the entire channel range of the MCA. Once the MCA was calibrated this process was repeated for other distances and radionuclides.

After applying calibration to the acquired spectra, counts measured per gamma-ray emission were obtained by utilizing regions of interests (ROIs). The ROIs are designated at the start and end of the peak for a given gamma-ray emission. By assigning ROIs, the software is able to calculate the area under the associated peak and calculate the counts for the specific energy peak such as net rate (counts/s), net area (total counts), centroid, full-width half max (FWHM), uncertainty, and gross area. Net count rate and uncertainty were utilized to obtain detector efficiency and associated error. The ratio of measured counts and source emission rate is proportional to efficiency as described in Eq. 1.

$$\varepsilon(\mathrm{E}) = \frac{\text{Net Rate(E)}}{\mathrm{A_m I_\gamma(E)}} \pm \frac{\text{Uncertainty(E)}}{\mathrm{A_m I_\gamma(E)}} \qquad (1)$$

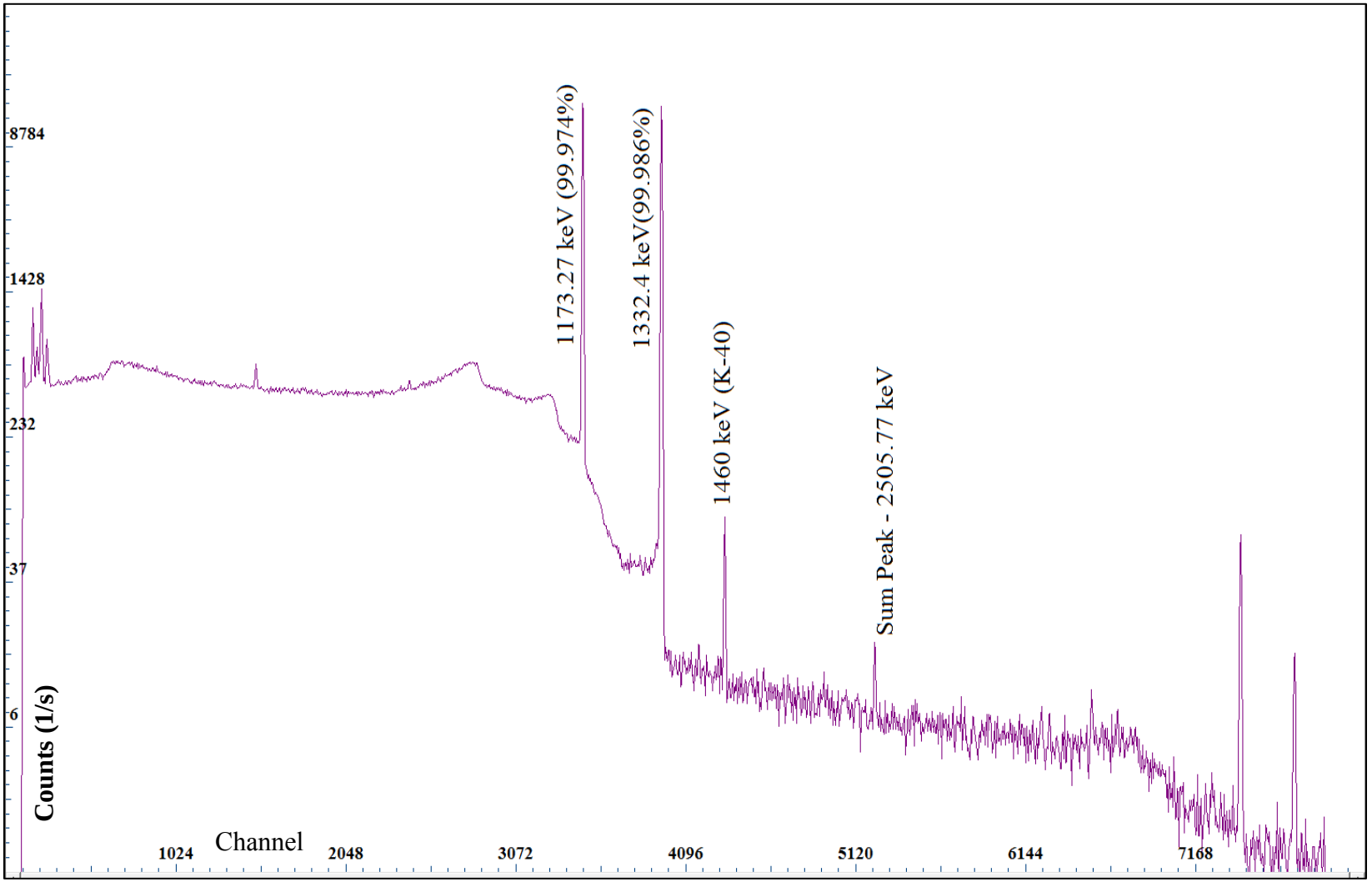

Figure 11. Un-calibrated Co-60 spectrum at 10 cm (Counts v. Channel Number).

In Eq.1, ε denotes efficiency, A_m is the decay corrected activity at time of measurement (source emission rate), and I_γ is the emission intensity of gamma-ray, also known as branching ratio. Efficiency, emission intensity, net count rate and uncertainty are dependent on incident gamma-ray energy. Initial activity for each source was decay corrected, from the calibration date of April and May 1998, by applying Eq. 2,

$$A_m = A_o e^{-\lambda t} \quad (2)$$

where A_o, denotes initial calibrated activity of the source when it was manufactured and certified, A_m is the decay corrected activity, λ is the physical decay constant for the particular radionuclide, and t denotes elapsed time from time of certification of the source activity to the time of measurement. Figure 12 provides a plot of efficiency versus energy as a function of distance for the HPGe detector utilized. Additional data regarding the calibration and efficiency of the HPGe detector is given in Appendix A.

Efficiency for a specific energy range can be calculated obtaining a curve which best fits the acquired data. Since spectra for each source was obtained separately and to minimize error propagation, efficiency curves were obtained based on Eu-152 gamma-ray emissions for all distances by applying the power fit [27]. Fitting a power polynomial function to the efficiency data results in high errors for energies below 150 keV due to the knee effect that occurs in p-type HPGe detectors as the one being utilized in this experiments. This effect is induced due to low energy photon absorption as they pass through the dead layer of the outer contact (crystal housing) of the detector. However, the power trend line provides excellent results for energy ranges above 120

keV. The efficiency curve at 20 cm obtained using Eu-152 is presented in Figure 13 and the Eu-152 spectrum is shown in Figure 14.

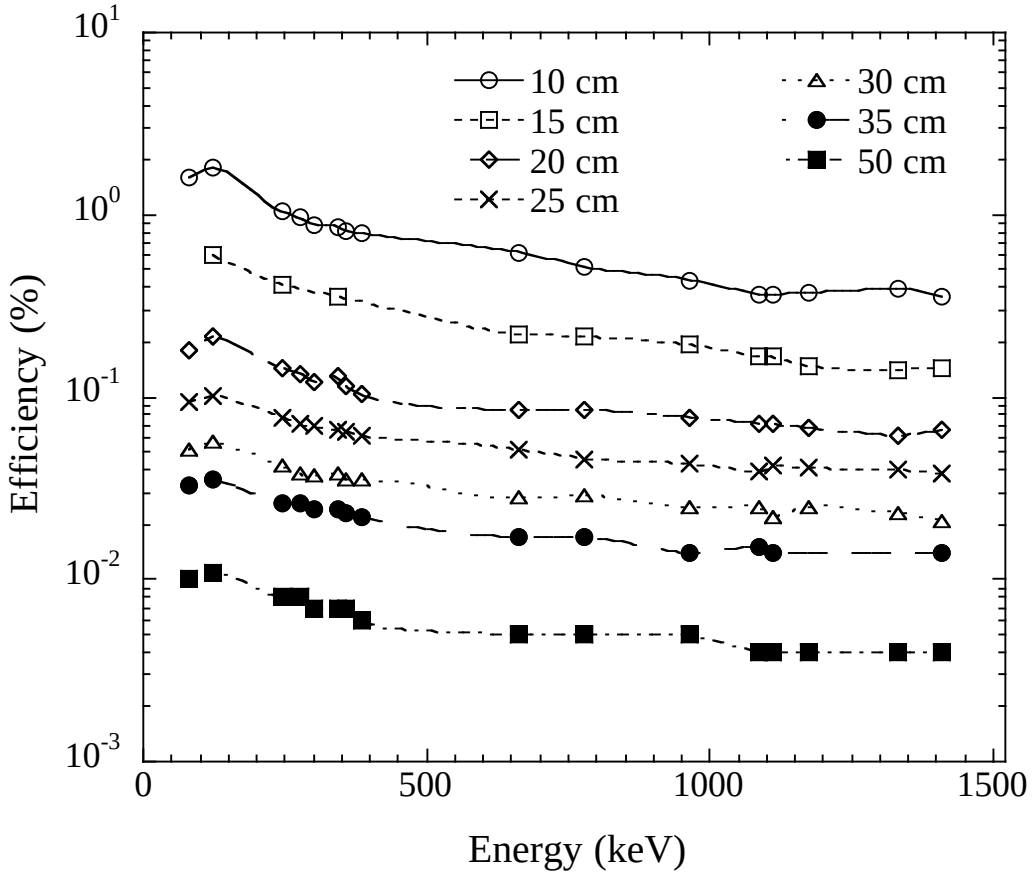

Figure 12. HPGe efficiency curves utilized for gamma-ray spectroscopy at different source distances.

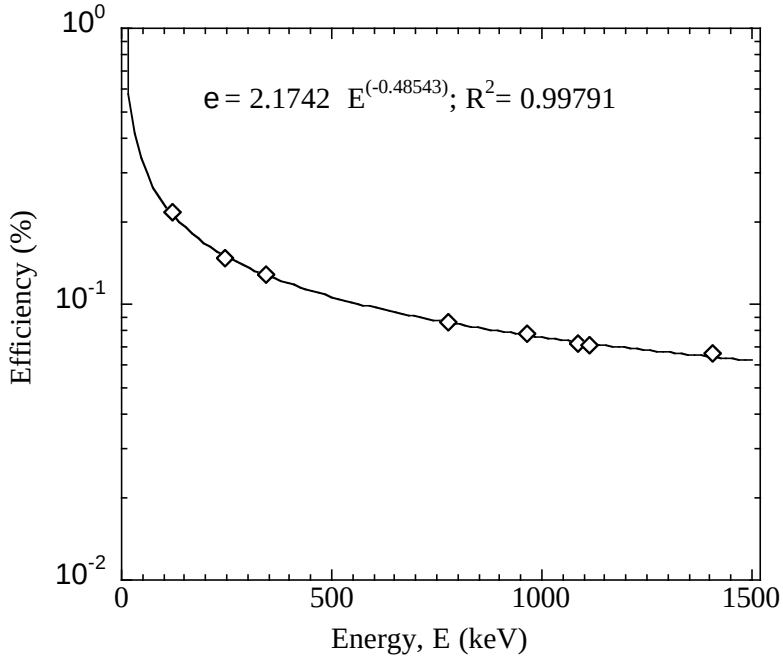

Figure 13. HPGe efficiency curve obtained using Eu-152 at 20 cm.

2.6 Gamma-ray Spectroscopy

Assessment of At-211 yield was performed utilizing activation analysis based on the principles of gamma-ray spectroscopy. Activation analysis is the process of determining activity of a daughter radionuclide based on the measurement of gamma-ray emission during decay. During bombardment of the Bi-209 target with alpha-particles, the Bi-209(α,2n)At-211 reaction accumulate activity of At-211. The rate of production of At-211 depends on the net sum of the production and decay rates as specified in Eq. 3 [46].

$$\frac{dN}{dt} = \phi_o \Sigma_{\alpha,2n} - \lambda N \quad (3)$$

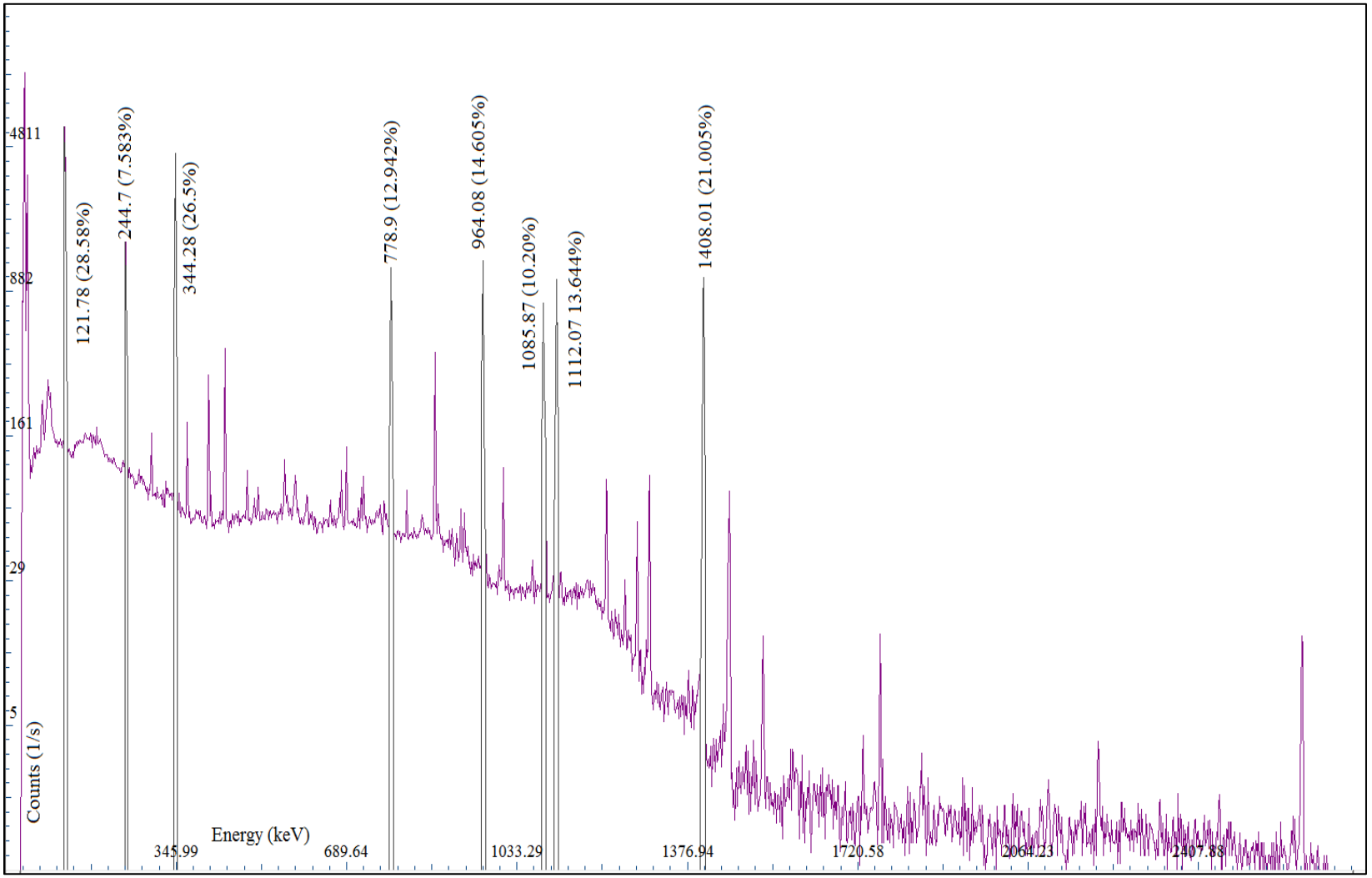

Figure 14. Eu-152 spectrum (20 cm) utilized to obtain detector efficiency.

The rate of decay specified in Eq. 3 is given by the term λN where λ is the physical decay constant and N is the total number of radioactive nuclei present at a given time. The production term is given by $\phi_o\Sigma_{(\alpha,2n)}$, where the alpha-particle flux is represented by ϕ_o and $\Sigma_{(\alpha,2n)}$ defines the activation reaction cross-section, which is averaged over the alpha-particle spectrum between 22 MeV and E_{max}. Solving Eq. 3 for the production term yields a first order ordinary differential equation with constant coefficients, Eq. 4.

$$\frac{dN}{dt} + \lambda N = \phi_o \Sigma_{\alpha,2n} \tag{4}$$

Solution to Eq. 4 can be obtained if the following assumptions are made [46]:

1. Constant alpha-particle flux.
2. Neglect burn-up of daughter atoms (do not get activated).
3. Neglect loss of target atoms.
4. No daughter atoms at t = 0 (N = 0).

Based on these assumptions and initial condition of N = 0 at t = 0, solution for Eq. 4 can be obtained, Eq. 5.

$$\mathrm{N(t)} = \frac{\phi_o \Sigma_{\alpha,2n}}{\lambda}(1 - \mathrm{e}^{-\lambda t}) \tag{5}$$

The exponential term in Eq. 5, accounts for the radioactive decay of the daughter atom during the activation process. By multiplying both sides of Eq. 5 with the decay constant, λ, activity for the daughter radionuclide can be obtained, Eq. 6.

$$\mathrm{A(t)} = \phi_o \Sigma_{\alpha,2n}(1 - \mathrm{e}^{-\lambda t}) \tag{6}$$

If physical decay is neglected, the saturation activity, A_∞, can be obtained at t = ∞ (Figure 15). However, for this study we had constant flux at the target but not through

the target. The target was utilized as a beam stop; therefore, to calculate saturation activity, the attenuation of the flux as a function of depth within the target must be determined. Being able to characterize the attenuation of the flux within the target is extremely difficult and therefore it was not performed. Consequently, the saturation activity was calculated experimentally using the principles of gamma-ray spectroscopy.

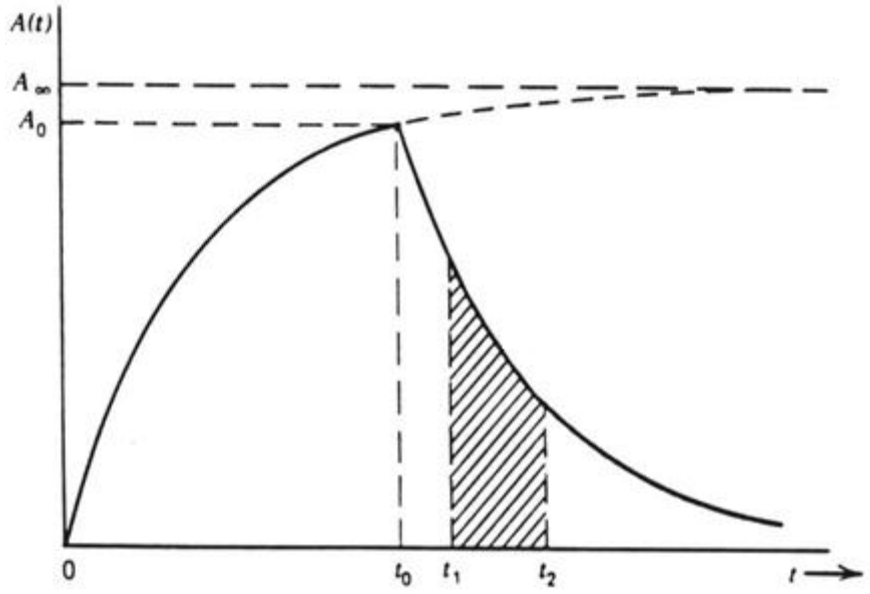

Figure 15. Plot of induced and saturation activity as a function of time [46].

From Figure 15, principles of activation detectors can be applied to measure and calculate activity of the daughter atoms at end of bombardment (EOB). In Figure 5, t_o denotes time of bombardment, t_1 is time when measurement is initiated, and t_2 is end of

measurement. The measured counts acquired between time interval t_1 to $t_2$can be obtained based on Eq. 7 [46].

$$C = \varepsilon \int_{t_1}^{t_2} A_o e^{-\lambda(t-t_o)} dt + B \quad (7)$$

$$C = \varepsilon \left(\frac{A_o}{\lambda}\right) e^{-\lambda t_o} \left(e^{-\lambda t_1} - e^{-\lambda t_2}\right) + B \quad (8)$$

In Eq. 7, C is the observed counts, B is the background counts, and A_o is the activity produced at EOB, and ε is the absolute efficiency of the detector system. From acquired measurements of the radiative emissions (gamma-rays) of the daughter atoms, both activity at EOB, $A(t_o)$, and saturation activity, A_∞, can be calculated by applying Eq. (9) and (10) respectively [46].

$$A_o = \frac{\lambda(C-B)}{\varepsilon_\gamma I_\gamma e^{\lambda t_o}\left(e^{-\lambda t_1} - e^{-\lambda t_2}\right)} \quad (9)$$

$$A_\infty = \frac{\lambda(C-B)}{\varepsilon_\gamma I_\gamma (1-e^{-\lambda t_o}) e^{\lambda t_o}\left(e^{-\lambda t_1} - e^{-\lambda t_2}\right)} \quad (10)$$

ε_γ is the efficiency of the gamma-ray as a function of its energy and I_γ is the relative emission intensity.

2.7 Neutron Production

In preparation for production runs of At-211 required for distillation, neutron shielding assessment was performed. The shielding was developed to minimize neutron activation of equipment in the cyclotron vault. From the Bi-209(α,2n)At-211 reaction, it is known that recoil neutrons will be emitted. Also, there are other reactions that contribute to the production of these neutrons. Therefore, a TALYS simulation was performed for alpha-particle energies between 0 and 28 MeV bombarding a Bi-209 target. This simulation was performed to obtain the neutron emission rate per incident

alpha-particle along with the generated neutron spectrum. The neutron spectrum was then coupled to the Monte Carlo code MCNPX to assess the required shielding and estimate the corresponding neutron dose rates at the surface of the shielding. Table 16 and Figure 16 presents the cross-section data with respect to neutron emission. Figure 17 shows a plot of the neutron yield for the Bi-209(α,xn) reaction. The emitted neutron energy spectrum was estimated by summing over the energy range of the incident alpha-particles (Figure 18). This assumption accounts for attenuation of the beam through the Bi-209 target when considering shielding requirements.

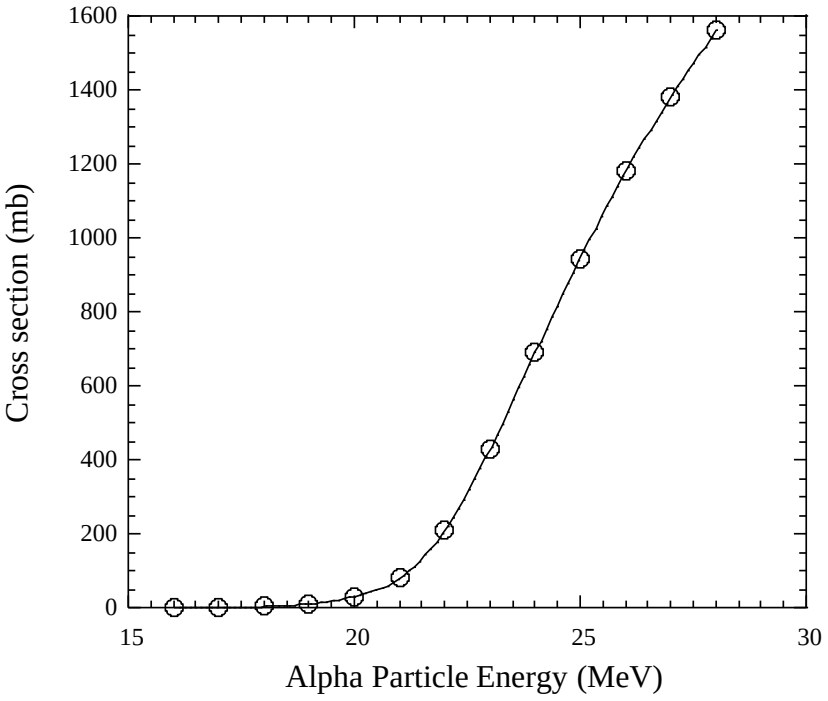

Figure 16. Neutron production cross-section for Bi-209(α,xn) reaction as a function of incident alpha-particle energy estimated using the code TALYS.

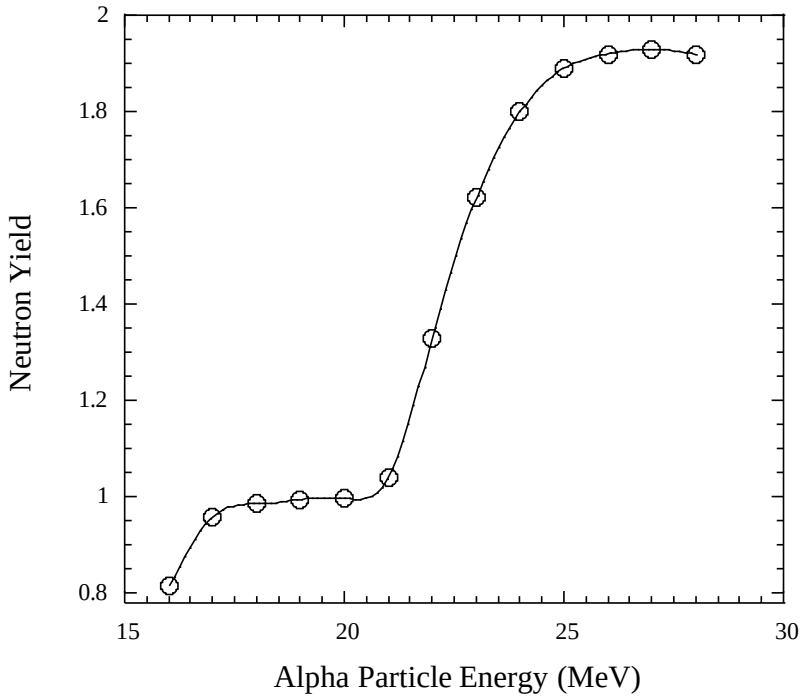

Figure 17. Neutron yield for Bi-209(α,xn) reaction per incident alpha-particle energy.

Table 16. Neutron production data for Bi-209(α,xn) reaction.

$Energy_{\alpha}$ (MeV)	Cross-section (mb)	Yield
16	0.15	0.81
17	0.74	0.96
18	2.89	0.98
19	10.00	0.99
20	30.20	1.00
21	79.13	1.04
22	208.85	1.33
23	428.38	1.62
24	689.73	1.80
25	944.92	1.89
26	1176.47	1.92
27	1383.23	1.93
28	1561.23	1.92

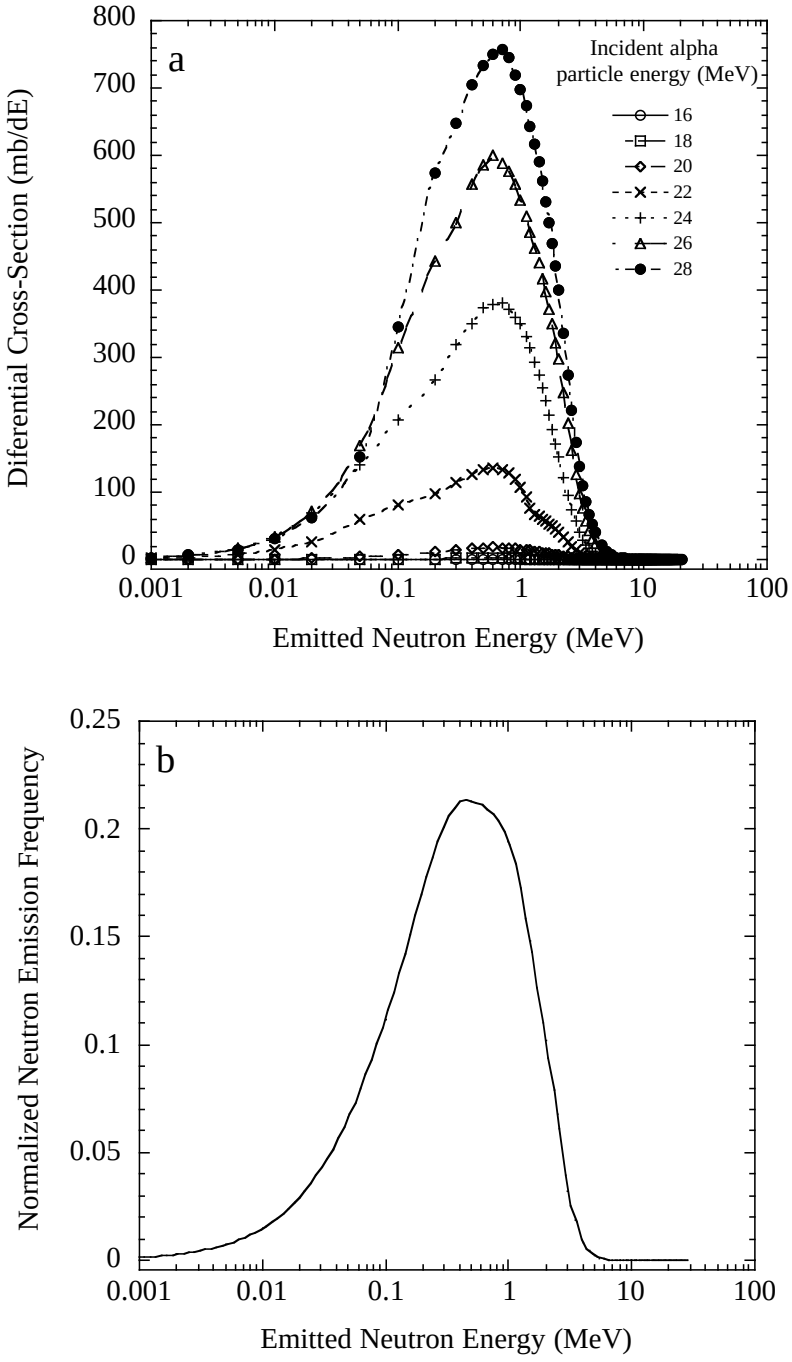

Figure 18. a) Differential cross-section of neutron production as a function of incident alpha-particle energy. b) Normalized neutron energy spectrum for Bi-209(α,xn) reaction from TALYS.

Based on TALYS analysis, the normalized neutron energy spectrum was utilized as the source energy spectrum for the MCNPX simulations. The MCNPX simulation was performed with and without shielding. From Figure 18 the mean energy of the neutron spectrum was calculated to be approximately 1.2 MeV. From the initial MCNPX simulations without shielding, we modeled a 2-inch borated polyethylene (5% boron) shielding to assess the reduction in neutron flux [47, 48]. Figure 19 represents the schematic utilized for the MCNPX simulations. In the simulation several tallies were utilized to obtain flux and dose rate values of neutrons and neutron induced photons. The geometrical placement of the neutron dose tallies in MCNPX was determined through discussions with Dr. Gabriel Tabacaru. Dose rates were obtained through the conversion of neutron and photon flux based on flux-to-dose rate tally modifiers within MCNPX, based on the International Commission on Radiological Protection (ICRP) 21 report [49]. MCNPX input files for the simulations can be found in Appendix B.

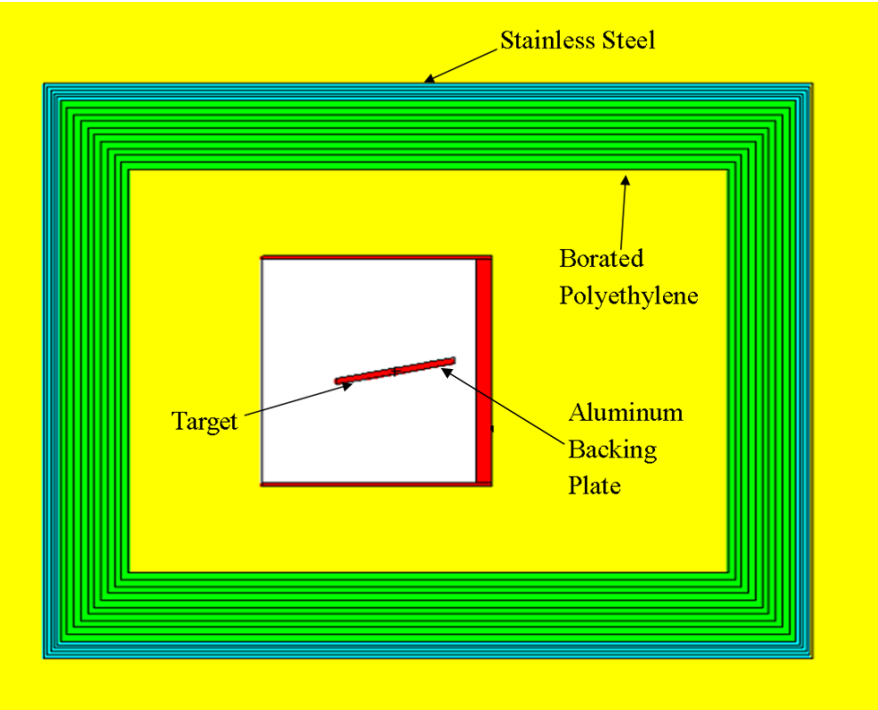

Figure 19. Target geometry utilized for MCNPX shielding simulations.

3. RESULTS AND DISCUSSION

3.1 Results

Production of At-211 was performed with two experiments. Both experiments utilized the target system and principles described in Section 2. The first experiment established the production of At-211 at the Texas A&M Cyclotron Institute. The success of the initial experiment led to the second experiment, where the production of contaminants was analyzed along with production optimization of At-211. Table 17 lists the parameters utilized for both experiments. Based on the given parameters for the experiments and principles of gamma-ray spectroscopy, assessment of At-211 was performed as described in Section 2.6.

Table 17. Experiment parameters for production of At-211 experiments using the K500 cyclotron.

Parameter	Experiment 1	Experiment 2
Bombardment Time (t_o)	4 h	4 h
Cooling time (t_o - t_1)	1.42 h	12.4 h
Measured time (t_1 -t_2)	1 h	1 h
Beam Intensity	163.17 nA	96.13 nA

Since the objective of initial experiment was to establish the feasibility of producing At-211, a nominal alpha particle beam energy of 27.8 MeV was selected. This energy was based on recommendations obtained from the open literature, which is optimal for production of At-211 and residual radionuclides. For the second experiment

the beam energy was estimated at 25.3 MeV as described in Section 2. Gamma-ray spectroscopy was carried out at 35 and 20 cm away from the HPGe detector for Experiment 1 and 2 respectively. After performing energy calibration on the acquired gamma-ray spectra, the peaks of all measured gamma-ray emissions were identified (Figures 20 and 21). These emissions help identify the radionuclide At-211 and other contaminants. Based on principles of gamma-ray spectroscopy discussed in Section 2.6, activity for the various gamma-ray emissions for all produced radionuclide was calculated. Table 18 and 19 represent all identified products paired with their gamma-ray emissions and their respective activities. Based on these principles, the average measured activity for the first experiment for At-211 was 23.48 ± 0.81 MBq with At-210 activity of 0.55 ± 0.07 MBq (<2.5% relative to At-211). Activity yields for the second experiment were less than that for the first experiment; however, production of At-210 and Po-210 was avoided. Activity of At-211 for the second experiment was 4.76 ± 0.13 MBq. Saturation activity of At-211 for both experiments based on Eq. 10 was calculated to be 73.81 MBq and 14.96 MBq.

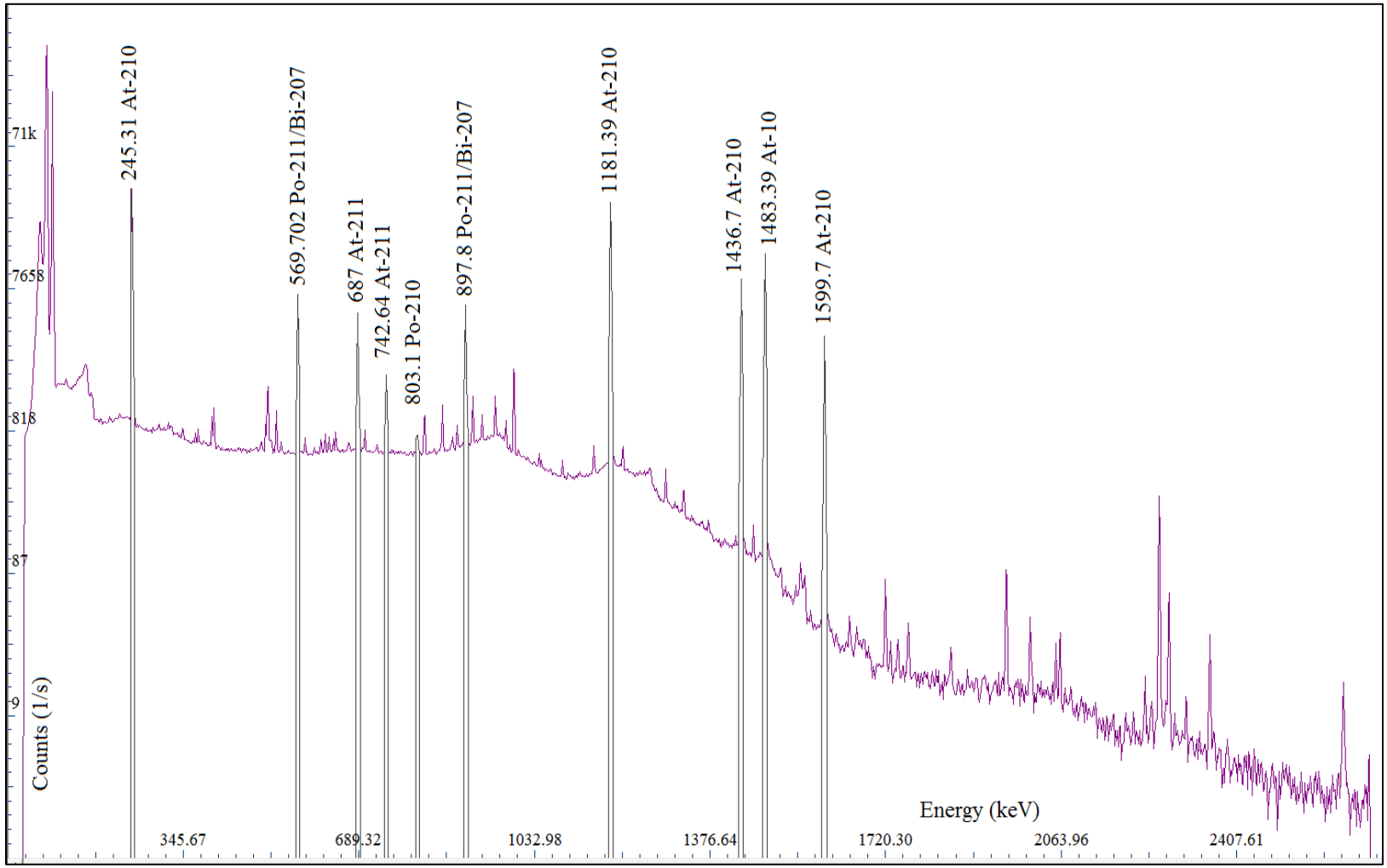

Figure 20. Gamma-ray spectrum based on first experiment measurement at 35 cm.

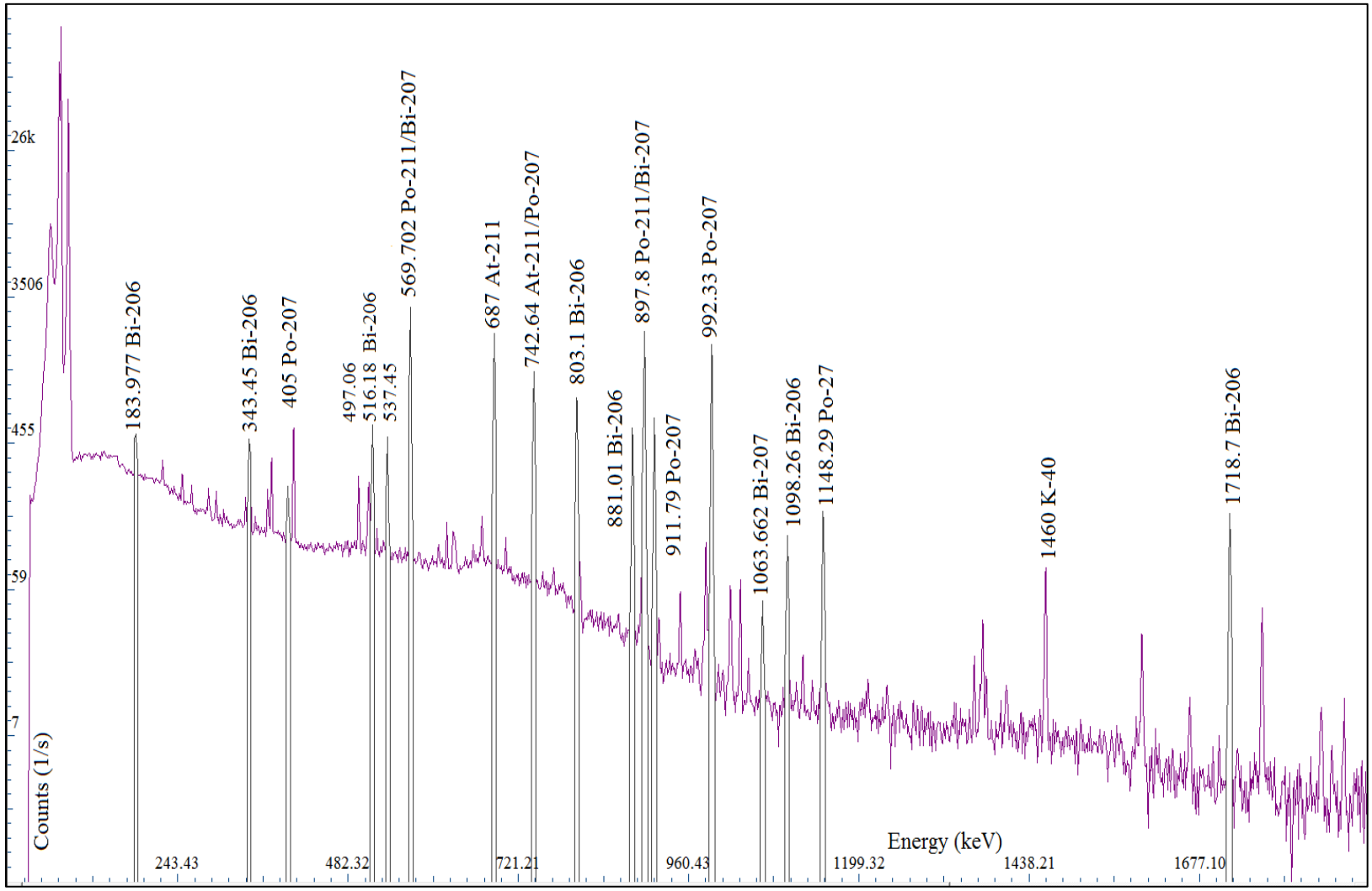

Figure 21. Gamma-ray spectrum based on second experiment measurements at 20 cm.

Table 18. Calculated production yields for the first experiment using an alpha-particle beam (27.8 MeV, 163.17 nA) measured at a distance of 35 cm from the detector.

Radionuclide	E_γ (keV)	I_γ (%)	half life	Peak Net Counts (Area)	Activity (MBq)	Activity (MBq/μAh)
At-211	687	0.261	7.241 h	31016	22.553	34.555
	742.64	0.001		-	-	-
Po-211*	569.702	29.10	0.516 s	39713	24.040	36.833
	897.8	32.65		36888	23.852	36.544
At-210	245.31	79	8.1 h	268566	0.420	0.643
	1181.39	99.3		251782	0.586	0.897
	1436.7	29		67115	0.578	0.885
	1483.39	46.5		108138	0.588	0.901
	1599.7	13.4		30118	0.586	0.897
Po-210**	803.1	0.00121	138.38 d	-	-	-
Bi-207***	569.702	97.74	31.55 y	-	-	-
	897.8	0.121		-		
	1063.662	74.5		-		
	1770.237	6.87		-		

*Po-211gamma-ray intensities are relative to decay of At-211 to Po-211.
** Po-210 activity is dependent on activity of At-210 at EOB.
***Bi-207 activity is a dependent on activity of At-211 at EOB.

Table 19. Calculated production yields for the second experiment using an alpha-particle beam (25.3 MeV, 96.13 nA) measured at a distance of 20 cm from the detector.

Radionuclide	Eγ (keV)	Iγ (%)	half life	Peak Net Counts (Area)	Activity (MBq)	Activity (MBq/μAh)
At-211	687	0.261	7.241	11483	4.610	11.990
	742.64	0.001		-	-	-
Po-211*	569.702	29.10	0.516 s	14759	4.852	12.618
	897.8	32.65		13165	4.813	12.518
Bi-207**	569.702	97.74	31.55 y	-	-	-
	1063.662	74.5		-		
	1770.237	6.87		-		
Bi-206	183.977	15.8	6.234 d	1023	0.001	0.003
	343.51	23.4		1193	0.001	0.003
	398	10.74		780	0.002	0.005
	497.06	15.31		959	0.002	0.005
	516.18	40.7		2646	0.002	0.005
	537.45	30.5		1952	0.002	0.005
	803.1	99		5862	0.002	0.005
	881.01	66.2		3850	0.002	0.006
	1718.7	31.8		2174	0.003	0.009
Po-207	405	9.7	5.8 h	2772	0.031	0.082
	742.64	28.2		-	-	-
	911.79	16.95		4153	0.040	0.104
	992.33	59.3		13193	0.038	0.099
	1148.29	5.72		1194	0.038	0.099

*Po-211gamma-ray intensities are relative to decay of At-211 to Po-211.
**Bi-207 activity is a dependent on activity of At-211 at EOB.

3.2 Discussion

The production yield for At-211 was calculated based on measured counts for the 687 keV gamma-ray emission and that of its daughter Po-211, which is extremely short-lived ($t_{1/2}$ = 0.516s). Due to Po-211 short half-life, the atoms of Po-211 which exists at the time of measurement are those that decay from At-211. Therefore, the half-life of Po-211 can be assumed to be similar to At-211, and its radiative emissions are normalized based on relative decay probability of At-211 via electron capture to Po-211 (58.2%). Activities for long lived radionuclides, such as Po-210 and Bi-207, were calculated based on the total number of parent atoms present at EOB and decay probability of the parent (branching ratio). Also, assessment of Po-210 activity is not possible via gamma-ray spectroscopy because Po-210 is a pure alpha-emitter. Therefore, the activity of Po-210 is assumed to be from the decay of At-210 via electron capture (99.82%).

Based on the gamma-ray spectrum for the first experiment, the radionuclide At-211 was observed. However, the radionuclides At-210 and P-210 were also observed. Based on cross-section evaluations in Section 2, the threshold energy for the production of At-210 is above 29 MeV and it should not have been produced. The production of these contaminants can be attributed to the use of stacked foil target system. When utilizing multiple stacked foils for beam degradation, the full-width half max (FWHM) of the beam has been shown to greatly increase [36]. The increase of the FWHM of the beam broadens the energy range of the alpha-particles reaching the Bi-209 target above the 29 MeV thresholds, thus enabling the production of At-210 and Po-210. The

experiment was deemed successful despite production of these contaminants because the total measured activity at EOB of At-210 was 0.55 ± 0.07 MBq. The content of At-210 produced was less than 2.5% of At-211 yield, which is consistent to observations in published literature [28, 29, 36]. In terms of distillation, in published literature it is observed that Po-210 activity was less than 0.02% of the At-211 activity collected and is not considered as the primary contaminant. Due to similar chemical properties of At-210 and At-211, At-210 is considered the primary contaminant to avoid.

Since the first experiment yielded the contaminants At-210 and Po-210, the second experiment was conducted to show that production of these contaminants could be further minimized or avoided completely. From the gamma-ray spectrum of the second experiment, production of At-210 and Po-210 was completely avoided. However, the production yield of At-211 was reduced by approximately 50%. This reduction in yield of At-211 is not desirable when distillation of At-211 is accounted. Based on published literature distillation can lead to a loss of up to 40 – 75% of the EOB At-211 activity [28, 29]. The reduction in yield of At-211 can be explained by low current extracted for the second experiment 96.13 nA compared to 163.17 nA of the first experiment. The cited reason was on going mechanical issues with the cyclotron.

However, production of contaminants was not completely avoided in the second experiment. In Table 17 it is shown that Bi-206 and Po-207 were both produced with yields of less than 0.04% and 0.8% relative to the At-211 yield, respectively. Based on these relative yields, Po-207 is considered the primary contaminant. The production channel for Po-207 was not identified.

3.3 Neutron Shielding

From MCNPX simulations, the dose rate was calculated based on emitted neutron spectra and induced photons (n, p) (Table 20). The actual dose rate during the experiment is proportional to the intensity of the alpha-particle beam extracted and the integral neutron yield of the beam energy through the target. From the simulations it is shown that neutron transmission is reduced by a maximum factor of 2.2. This value is comparable to those found in published literature [46]. Based on these calculations a shielding cart was developed based on the geometry of the simulation. The walls of the cart were layered with four inches of borated polyethylene and covered with an external plane of stainless-steel of 0.5 inches (Figure 22).

Table 20. MCNPX contact dose rate projections for neutrons and induced photons.

Tally Type	x	y	z	Dose rate without shielding (Sv/h)	Dose rate with shielding (Sv/h)
Neutron	23	0	0	1.42E-10	6.29E-11
Photon				2.74E-14	4.71E-13
Neutron	-23	0	0	1.30E-10	5.97E-11
Photon				2.58E-14	4.50E-13
Neutron	0	10	-33	4.26E-11	1.92E-11
Photon				1.24E-14	2.56E-13
Neutron	0	-10	-33	4.25E-11	2.02E-11
Photon				1.25E-14	2.69E-13
Neutron	10	0	-33	5.73E-11	2.48E-11
Photon				1.24E-14	2.61E-13

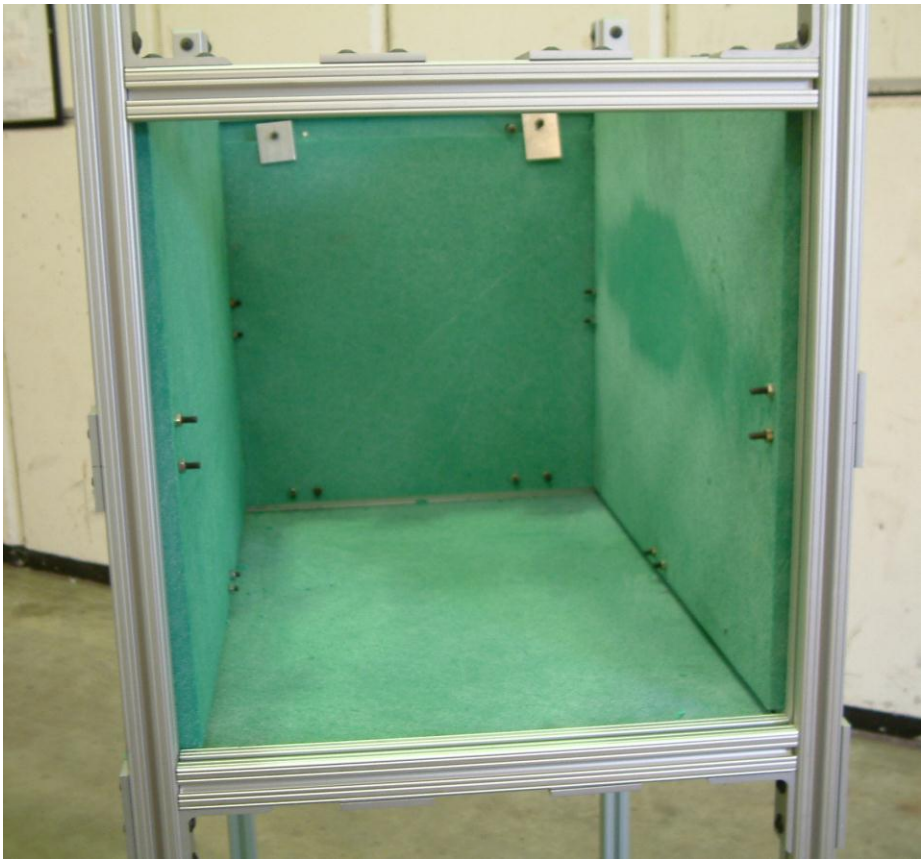

Figure 22. Borated-polyethylene shielding cart designed to reduce neutron transmission during the irradiation of bismuth-209 with alpha-particles.

4. SUMMARY AND RECOMMENDATIONS

4.1 Conclusion

The production of At-211 was established through two experiments at the Texas A&M Cyclotron Institute. In preparation for these experiments, numerous preliminary computational studies were carried out and analyzed the initial production of At-211. These studies include cross-section evaluations, beam degradation analysis, target development, and HPGe detector calibration. Based on these studies, it was proven that At-211 could be produced at the Texas A&M Cyclotron Institute while minimizing and controlling the production of contaminants, mainly At-210.

The following are observations and results obtained from the two experiments:

1. At-211 yields were 35.98 and 12.38 MBq/(μA-h) based on principles of gamma-ray spectroscopy. Saturation activity of At-211 for each experiment was calculated to be 73.84 MBq and 14.96 MBq.
2. Contaminants yields were less than 0.9% relative to At-211 activity except for At-210 which was less than 2.5% of At-211, and with lower beam energy production of At-210 and Po-210 was avoided.

The following are recommendations for future research into this area:

1. Production of At-211 should be assessed through direct bombardment of Bi-209.
2. Use of silicon detectors to characterize the initial beam extracted so FWHM calculations can be performed.

3. Production of At-211 should be characterized with experiments utilizing the K150 cyclotron.
4. Different software for gamma-ray spectroscopy should be utilized. The AMPTEK software had a tendency to crash during analysis as it requires significant amount of computing resources.

4.2 Future Work

The successful production of At-211 will allow the continuation of future research in the area of TRT. Future goals included the production of At-211 for distillation purposes, development of radioactive nanoparticles, and functionalization with monoclonal antibodies and other biological compounds. In order to produce the activity of At-211 required for distillation, a new target was developed. Development of this target was stimulated by the concerns of melting the Bi-209 target foil during bombardment. This concern arose due to the use of K150 cyclotron beam which can deliver higher beam intensity. The energy profile of the extracted K150 beam is extremely discrete with a small FWHM of less than 2%. These properties of the K150 cyclotron make it an ideal production source; however, the high intensity equates to dissipation of higher energies by the Bi-209 target.

The dissipation of alpha-particle beam energy requires an active cooling system for the target to prevent the melting of bismuth (the melting point of bismuth is 271 ^{o}C). An aluminum block target was designed to withstand the heat produced during bombardment. This design was developed by Dr. Larsen at Duke University [29]. The dimensions of the aluminum target were 9 cm by 2 cm by 0.5 cm and a groove of 100

μm was machined on the top layer for the direct deposition of bismuth (Figure 22). This groove was developed to deposit melted bismuth (Sigma-Aldrich, 99.99% purity). This target was also machined at the bottom to generate a u-shape and have two thin fins that are in contact with the target holder and cooling system. This shape was deemed best suited to dissipate the heat. The aluminum target for At-211 distillation experiments is designed to be mounted onto a target holder with a coolant channel. The target holder was developed and designed at the Texas A&M Cyclotron Institute (Figures 23 and 24). The coolant channel will be utilized to cool the aluminum target and prevent the melting of bismuth.

Figure 23. Aluminum target with groove designed to dissipate heat produced during the bombardment of melted bismuth.

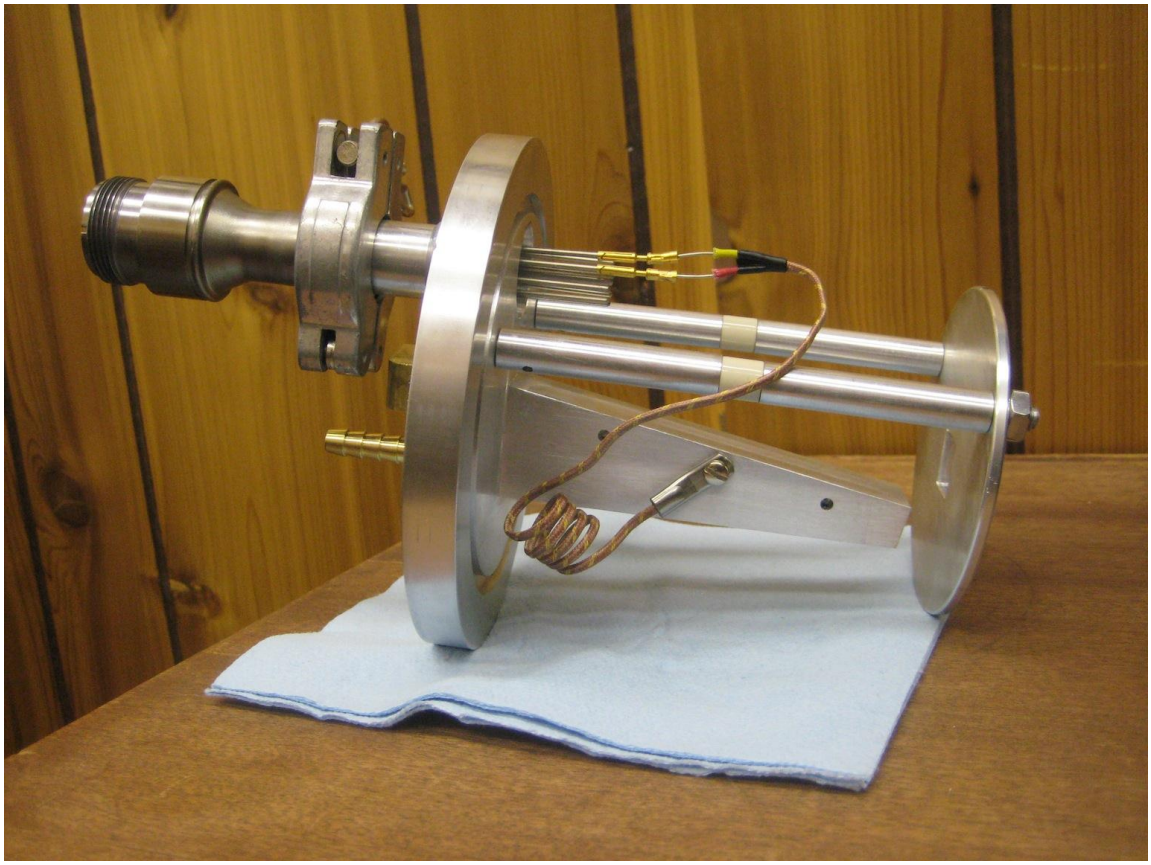

Figure 24. Redesigned target holder for the production of At-211 for distillation experiments.

REFERENCES

[1] Altekruse SF, Kosary CL, Krapcho M, Neyman N, Aminou R, Waldron W, Ruhl J, Howlader N, Tatalovich Z, Cho H, Mariotto A, Eisner MP, Lewis DR, Cronin K, Chen HS, Feuer EJ, Stinchcomb DG, Edwards BK (eds). Bethesda, MD, SEER Cancer Statistics Review, 1975-2008, National Cancer Institute. http://seer.cancer.gov/csr/1975_2008/.

[2] Speer TW. Targeted Radionuclide Therapy, Philadelphia: Lippincott Williams & Wilkins, 2011.

[3] Pressman D. Tissue localizing antibodies. Ann N Y Acad Sci 1955;59:376-80.

[4] Pressman D. Radiolabeled antibodies. Ann N Y Acad Sci 1957;69:644-50.

[5] Pressman D. The development and use of radiolabeled antitumor antibodies. Cancer Res 1980;40:2960-4.

[6] Pressman D, Korngold L. The *in vivo* localization of anti-Wagner-osteogenic-sarcoma antibodies. Cancer 1953;6:619-23.

[7] Pressman D, Watanabe T. Tumor localization of radiolabeled antibodies raised by a mouse plasma cell tumor. Immunochemistry 1975;12:581-4.

[8] Nungester WJ, Fisher H. The inactivation *in vivo* of mouse lymphosarcoma 6C3HED by antibodies produced in a foreign host species. Cancer Res 1954;14:284-8.

[9] Nungester WJ, Garrison D, Fuller D, Hartman RS. Assay of antitumor properties of serum. Med Bull 1955;21:365-70.

[10] Kohler G, Milstein C. Continuous cultures of fused cells secreting antibody of predefined specificity. Nature 1975;256:495-7.

[11] Jacene HA, Filice R, Kasecamp W, Wahl RL. Comparison of ^{90}Y-ibritumomab tiuxetan and ^{131}I-tositumomab in clinical practice. J Nucl Med 2007;48:1767-76.

[12] Zalutsky MR, Reardon DA, Pozzi OR, Vaidyanathan G, Bigner DD. Targeted alpha-particle radiotherapy with ^{211}At-labeled monoclonal antibodies. Nucl Med Biol 2007;34:779-85.

[13] Volkert WA, Hoffman TJ. Therapeutic radiopharmaceuticals. Chem Rev 1999;99:2269-92.

[14] Larsen RH, Vaidyanathan G, Zalutsky MR. Cytotoxicity of alpha-particle-emitting 5-[^{211}At]astato-2'-deoxyuridine in human cancer cells. Int J Radiat Biol 1997;72:79-90.

[15] Sgouros G. Alpha-particles for targeted therapy. ADDR 2008;60:1402-6.

[16] Akabani G, Carlin S, Welsh P, Zalutsky MR. *In vitro* cytotoxicity of ^{211}At-labeled trastuzumab in human breast cancer cell lines: effect of specific activity and HER2 receptor heterogeneity on survival fraction. Nucl Med Biol 2006;33:333-47.

[17] Andersson H, Elgqvist J, Horvath G, Hultborn R, Jacobsson L, Jensen H, et al. Astatine-211-labeled antibodies for treatment of disseminated ovarian cancer: an overview of results in an ovarian tumor model. Clin Cancer Res 2003;9:3914S-21S.

[18] Bloomer WD, McLaughlin WH, Lambrecht RM, Atcher RW, Mirzadeh S, Madara JL, et al. ^{211}At radiocolloid therapy: further observations and comparison with radiocolloids of ^{32}P, ^{165}Dy, and ^{90}Y. Int J Radiat Oncol Biol Phys 1984;10:341-8.

[19] Larsen RH, Hoff P, Vergote IB, Bruland OS, Aas M, De Vos L, et al. Alpha-particle radiotherapy with ^{211}At-labeled monodisperse polymer particles, ^{211}At-labeled IgG proteins, and free ^{211}At in a murine intraperitoneal tumor model. Gynecol Oncol 1995;57:9-15.

[20] Lindegren S, Frost S, Back T, Haglund E, Elgqvist J, Jensen H. Direct procedure for the production of ^{211}At-labeled antibodies with an epsilon-lysyl-3-(trimethylstannyl)benzamide immunoconjugate. J Nucl Med 2008;49:1537-45.

[21] Palm S, Andersson H, Back T, Claesson I, Delle U, Hultborn R, et al. *In vitro* effects of free ^{211}At, ^{211}At-albumin and ^{211}At-monoclonal antibody compared to external photon irradiation on two human cancer cell lines. Anticancer Res 2000;20:1005-12.

[22] Pozzi OR, Zalutsky MR. Radiopharmaceutical chemistry of targeted radiotherapeutics, Part 2: radiolytic effects of ^{211}At alpha-particles influence N-succinimidyl 3-^{211}At-astatobenzoate synthesis. J Nucl Med 2005;46:1393-400.

[23] Zalutsky MR, Pozzi OR. Radioimmunotherapy with alpha-particle emitting radionuclides. Q J Nucl Med Mol Imaging 2004;48:289-96.

[24] Zalutsky MR, Reardon DA, Akabani G, Coleman RE, Friedman AH, Friedman HS, et al. Clinical experience with alpha-particle emitting ^{211}At: treatment of recurrent

brain tumor patients with ^{211}At-labeled chimeric antitenascin monoclonal antibody 81C6. J Nucl Med 2008;49:30-8.

[25] Zalutsky MR, Vaidyanathan G. Astatine-211-labeled radiotherapeutics: an emerging approach to targeted alpha-particle radiotherapy. Curr Pharm Des 2000;6:1433-55.

[26] Zalutsky MR, Zhao XG, Alston KL, Bigner D. High-level production of alpha-particle-emitting ^{211}At and preparation of ^{211}At-labeled antibodies for clinical use. J Nucl Med 2001;42:1508-15.

[27] Hermanne A, Tarkanyi F, Takacs S, Szucs Z, Shubin YN, Dityuk AI. Experimental study of the cross-sections of alpha-particle induced reactions on ^{209}Bi. Appl Radiat Isot 2005;63:1-9.

[28] Lambrecht RM, Mirzadeh S. Cyclotron isotopes and radiopharmaceuticals-XXXV astatine-211. Int. J. Appl. Radiat. Isot. 1984;36:443-50.

[29] Larsen RH, Wieland BW, Zalutsky MR. Evaluation of an internal cyclotron target for the production of ^{211}At via the ^{209}Bi (alpha,2n)^{211}At reaction. Appl Radiat Isot 1996;47:135-43.

[30] Morzenti S, Bonardi ML, Groppi F, Zona C, Persico E, Menapace E, et al. Cyclotron production of ^{211}At/^{211g}Po by ^{209}Bi(a,2n) reaction. Journal of Radioanalytical and Nuclear Chemistry 2008;276:843-7.

[31] Neirinckx RD, Smit JA. Separation of astatine-211 from bismuth metal. Anal Chim Acta 1973;63:201-4.

[32] Pozzi OR, Zalutsky MR. Radiopharmaceutical chemistry of targeted radiotherapeutics, Part 1: effects of solvent on the degradation of radiohalogenation precursors by ^{211}At alpha-particles. J Nucl Med 2005;46:700-6.

[33] Pozzi OR, Zalutsky MR. Radiopharmaceutical chemistry of targeted radiotherapeutics, Part 3: alpha-particle-induced radiolytic effects on the chemical behavior of ^{211}At. J Nucl Med 2007;48:1190-6.

[34] Schultz MK, Hammond M, Cessna JT, Plascjak P, Norman B, Szajek L, et al. Assessing the ^{210}At impurity in the production of ^{211}At for radiotherapy by ^{210}Po analysis via isotope dilution alpha spectrometry. Appl Radiat Isot 2006;64:1365-9.

[35] Chu SYF, Ekstrom LP, Firestone RB. WWW Table of Radioactive Isotopes, Online Database. LBNL Berkeley, CA; 1999. http://nucleardata.nuclear.lu.se/nucleardata/toi/

[36] Henriksen G, Messelt S, Olsen E, Larsen RH. Optimisation of cyclotron production parameters for the ^{209}Bi(alpha, 2n) ^{211}At reaction related to biomedical use of ^{211}At. Appl Radiat Isot 2001;54:839-44.

[37] Lebeda O, Jiran R, Ralis J, Stursa J. A new internal target system for production of ^{211}At on the cyclotron U-120M. Appl Radiat Isot 2005;63:49-53.

[38] Lindegren S, Back T, Jensen HJ. Dry-distillation of astatine-211 from irradiated bismuth targets: a time-saving procedure with high recovery yields. Appl Radiat Isot 2001;55:157-60.

[39] Youngblood DH. The Texas A&M K500 cyclotron facility. Nuclear Instruments, Methods in Physics Research 1991;B56:991 - 5.

[40] Tribble R. A proposed uacility upgrade for the Texas A&M University Cyclotron Institute. Internal Report, College Station, TX 2001.

[41] Agency IAEA. Cyclotron produced radionuclides: physical characteristics, production pethods: Technical Reports Series No. 468. 2009, p. 33 - 40.

[42] Koning A, Hilaire S, Duijvestijn M. TALYS. Software Manual, NRG; 2008. http://www.talys.eu/

[43] Ramler WJ, Wing J, Henderson DJ, Huizenga JR. Exictation Functions of Bismuth, Lead. Physical Review 1959;114:154 - 62.

[44] Ziegler J. SRIM & TRIM. Software, 2011. http://www.srim.org/

[45] Group L. LISE++: a simulation of fragment separators. Software, NSCL/MSU, 2011. http://groups.nscl.msu.edu/lise/lise.html

[46] Knoll GF. Radiation Detection, Measurement, New York: Wiley,2000.

[47] Allen FJ, Futterer AT, Wright WP. Neutron Transmission versus Thickness for Some Common Materials. Internal Report, Aberdeen Proving Ground Bethesda, MA, 1962.

[48] Wuest CR. TART Calculations of Neutron Attenuation, Neutron-induced Photons on 5%, 20% Boraded Polyethylene Slabs. Lawrence Livermore National Laboratory. Livermore, CA; 1992.

[49] Ford MR. Report of the Task Group on Dose Calculations to ICRP Committee 2, March 17-21, 1980; Department of Enegry, Oak Ridge National Laboratory. Oak Ridge, TN 1980.

APPENDIX A

DETECTOR EFFICIENC AND CALIBARTION DATA

Table A.2. HPGe efficiency values as a function of source to detector distance based on Co-60, Ba-133, Cs-237, and Eu-152.

Energy (keV)	Efficiency (%)						
	SDD 10 cm	SDD 15 cm	SDD 20 cm	SDD 25 cm	SDD 30 cm	SDD 35 cm	SDD 50 cm
80.9971	1.591	-	0.182	0.094	0.052	0.033	0.010
121.7817	1.805	0.606	0.215	0.102	0.057	0.035	0.011
244.6975	1.046	0.414	0.146	0.078	0.042	0.026	0.008
276.398	0.961	-	0.135	0.071	0.038	0.026	0.008
302.853	0.878	-	0.121	0.069	0.037	0.024	0.007
344.2785	0.860	0.356	0.129	0.066	0.038	0.024	0.007
356.017	0.823	-	0.114	0.065	0.035	0.023	0.007
383.851	0.796	-	0.104	0.062	0.035	0.022	0.006
661.657	0.623	0.222	0.085	0.052	0.028	0.017	0.005
778.904	0.519	0.215	0.086	0.046	0.029	0.017	0.005
964.079	0.440	0.195	0.078	0.043	0.025	0.014	0.005
1085.869	0.367	0.167	0.072	0.039	0.025	0.015	0.004
1112.074	0.367	0.167	0.071	0.042	0.022	0.014	0.004
1173.273	0.375	0.149	0.068	0.041	0.025	-	0.004
1332.501	0.397	0.142	0.062	0.040	0.023	-	0.004
1408.006	0.359	0.146	0.066	0.038	0.021	0.014	0.004

APPENDIX B

INPUT FILES FOR MCNPX SIMULATION

MCNPX – Dose rates without shielding

Neutron Spectrum for 209-Bi(alpha,n) reaction - GT

```
c ===========================================================================
c CELL CARD
c ===========================================================================
10    1 -2.700   -10                $ Al Target Holder
11    2 -9.800   -11                $ 30 Micron Bi Target
12    1 -2.7     -12 -13 14           $ Target Holder Backing Plate
13    1 -2.7     -15 12 -16 14        $ Al Beam Line Pipe
14    3 -1.22E-7  10 11 -12 13 -16     $ Volume inside Pipe
17    3 -1.22E-3 -17 (-14:15:16)       $ air around the pipe
18    3 -1.22E-3   -18 17              $ air around the pipe
19    3 -1.22E-3   -19 18              $ air around the pipe
20    3 -1.22E-3   -20 19              $ air around the pipe
21    3 -1.22E-3   -21 20              $ air around the pipe
22    3 -1.22E-3   -22 21              $ air around the pipe
23    3 -1.22E-3   -23 22              $ air around the pipe
24    3 -1.22E-3   -24 23              $ air around the pipe
25    3 -1.22E-3   -25 24              $ air around the pipe
26    3 -1.22E-3   -26 25              $ air around the pipe
27    3 -1.22E-3   -27 26              $ air around the pipe
28    3 -1.22E-3    -28 27             $ air around the pipe
29    3 -1.22E-3    -29 28             $ air around the pipe
30    3 -1.22E-3    -30 29             $ air around the pipe
31    3 -1.22E-3    -31 30             $ air around the pipe
32    3 -1.22E-3    -32 31             $ air around the pipe
```

```
47    3 -1.22E-3 -90  32            $ Outside World
90    0         90                $ Void

c ===========================================================================
c SURFACE CARD
c ===========================================================================
10  1  rpp -0.25 0.25 -1 1 -4.5 4.5              $ Al block
11  1  rpp 0.25 0.253 -1 1 -4.5 4.5              $ Bismuth-209
12    cz  8.25                                  $ Al back plate cylinder
13    pz -6                                     $ Backing Plate Plane (Top)
14    pz -7.2                                   $ Backing Plate Plane (Bottom)
15    cz 8.55                                   $ Beam Line Pipe Cylinder
16    pz 10                                     $ Beam Line Pipe plane
17    rpp -15.00 15.00 -15.00 15.00 -24.92 20.00   $ 2" of Borated Polyethylene
18    rpp -15.51 15.51 -15.51 15.51 -25.43 20.51   $ 2" of Borated Polyethylene
19    rpp -16.02 16.02 -16.02 16.02 -25.94 21.02   $ 2" of Borated Polyethylene
20    rpp -16.52 16.52 -16.52 16.52 -26.44 21.52   $ 2" of Borated Polyethylene
21    rpp -17.03 17.03 -17.03 17.03 -26.95 22.03   $ 2" of Borated Polyethylene
22    rpp -17.54 17.54 -17.54 17.54 -27.46 22.54   $ 2" of Borated Polyethylene
23    rpp -18.05 18.05 -18.05 18.05 -27.97 23.05   $ 2" of Borated Polyethylene
24    rpp -18.56 18.56 -18.56 18.56 -28.48 23.56   $ 2" of Borated Polyethylene
25    rpp -19.06 19.06 -19.06 19.06 -28.98 24.06   $ 2" of Borated Polyethylene
26    rpp -19.57 19.57 -19.57 19.57 -29.49 24.57   $ 2" of Borated Polyethylene
27    rpp -20.08 20.08 -20.08 20.08 -30.00 25.08   $ 2" of Borated Polyethylene
28    rpp -20.33 20.33 -20.33 20.33 -30.25 25.33   $ 0.5" of SS Plate
29    rpp -20.59 20.59 -20.33 20.33 -30.51 25.59   $ 0.5" of SS Plate
30    rpp -20.84 20.84 -20.59 20.59 -30.76 25.84   $ 0.5" of SS Plate
31    rpp -21.10 21.10 -20.59 20.59 -31.02 26.10   $ 0.5" of SS Plate
32    rpp -21.35 21.35 -20.59 20.59 -31.27 26.35   $ 0.5" of SS Plate
90    so 300                          $ Tally ROI & Outside Environment
```

```
c ===========================================================================
c DATA CARD
c ===========================================================================
c Target Plate offset by 10 Degrees
*TR1 0 0 0 10 90 80 90 0 90 100 90 10
c
c Polyethylene Block Translocation
TR2 0 0 -30 1 0 0 0 1 0 0 0 1
TR3 -22.62 0 0 1 0 0 0 1 0 0 0 1
TR4 22.62 0 0 1 0 0 0 1 0 0 0 1
c
MODE N H D T P A S #
IMP:N 1 21R 0
IMP:P 1 21R 0
IMP:H 1 21R 0
IMP:D 1 21R 0
IMP:A 1 21R 0
IMP:T 1 21R 0
IMP:S 1 21R 0
IMP:# 1 21R 0
c
PHYS:N 100 0 0 -1 -1 0 2
PHYS:H 100 0 -1 J 0 J 1
PHYS:A 100 3j 0
PHYS:# 140 J J J 0
c
CUT:# J 0.01
CUT:H J 0.01
CUT:A J 0.01
CUT:D J 0.01
CUT:S J 0.01
```

```
CUT:N J 1e-9
c
LCA 2 1 1 23 1 1 0 1 0
c
sdef PAR=1 x=d1 y=d2 z=d3 CCC=11 ERG=d4 VEC=0 0 -1 DIR=d5 EFF=0.0001
SI1  -0.4 0.9
SP1  0 1
SI2 -1 1
SP2  0 1
SI3 -3.5 3.5
SP3  0 1
SI4 H 0 0.001 0.002 0.005 0.01 0.05 0.1 0.5 1 1.5 2 2.5 3 3.5 4 4.5 5 5.5 6 6.5
    7 7.5 8 8.5 9 9.5 10 10.5 11 11.5 12 12.5
SP4 D 0 0.001406153 0.002831182 0.007373327 0.014942203 0.066366757 0.112268423
    0.212833861 0.194489262 0.148338576 0.102227302 0.06804882 0.032269259
    0.018947065 0.008382303 0.004312252 0.002205652 0.001131632 0.000618138
    0.000351801 0.000223496 0.000145165 0.00010153 6.85231E-05 4.80271E-05
    3.03043E-05 1.97037E-05 1.02224E-05 5.99723E-06 1.82244E-06 1.22686E-06
    1.27672E-08
SI5  -1 9i 1
SP5   0 0.10 9r
SB5   0 0.02 8r 0.84
c ----
PTRAC cell=17 max=10000 TYPE=N FILE=asc
c ----
c Rectangular mesh
tmesh
rmesh1:N
cora1 -27 53i 27
corb1 -27 53i 27
corc1 -54 29i -24
```

```
rmesh11:P
cora11 -27 53i 27
corb11 -27 53i 27
corc11 -54 29i -24
endmd
c Detector tallies
F5:N 23 0 0 1
DF5 IU=1 IC=10
FC5 Neutron Dose on the side of the box +x
F15:P 23 0 0 1
DF15 IU=1 IC=10
FC15 Photon Dose on the side of the box +x
c
F25:N -23 0 0 1
DF25 IU=1 IC=10
FC25 Neutron Dose on the side of the box -x
F35:P -23 0 0 1
DF35 IU=1 IC=10
FC35 Photon Dose on the side of the box -x
c
F45:N 0 10 -33 1
DF45 IU=1 IC=10
FC45 Neutron Dose forward direction
F55:P 0 10 -33 1
DF55 IU=1 IC=10
FC55 Gamma Dose forward direction
c
F65:N 0 -10 -33 1
DF65 IU=1 IC=10
FC65 Neutron Dose forward direction for symmetry
F75:P 0 -10 -33 1
```

```
DF75 IU=1 IC=10
FC75 Gamma Dose forward direction for symmetry
c
F85:N 10 0 -33 1
DF85 IU=1 IC=10
FC85 Neutron Dose forward direction for symmetry
F95:P 10 0 -33 1
DF95 IU=1 IC=10
FC95 Gamma Dose forward direction for symmetry
c
c End Tally
m1     13027 -1.00
m2     83209 -1.00
c air internet 15 deg at sea level
m3 7014.66c -0.745962 8016.66c -0.228590 18000.42c -2.5448e-2 GAS=1
c 5% Borated Polyethylene
c Source:  TART LLNL
c Specified elemental Composition
c Total Mass Density :     0.936 g/cm^3
c
m4    1001 -0.11598
      1002 -0.00002
      5010 -0.0098
      5011 -0.0402
      6000 -0.612
      8016 -0.222
mt4 poly.10t
c
c SS Plate for Gammas
m5    26000 -0.9865
       6000 -0.0015
```

```
     25055 -0.0060
     14000 -0.0060
c ------------------------------------------------
NPS 1000000
c PRDMP 1E5 1E5
```

MCNPX – Dose rates with shielding

Neutron Spectrum for 209-Bi(alpha,n) reaction - GT

```
c ===========================================================================================
c CELL CARD
c ===========================================================================================
10    1 -2.700   -10               $ Al Target Holder
11    2 -9.800   -11               $ 30 Micron Bi Target
12    1 -2.7     -12 -13 14          $ Target Holder Backing Plate
13    1 -2.7     -15 12 -16 14       $ Al Beam Line Pipe
14    3 -1.22E-7  10 11 -12 13 -16    $ Volume inside Pipe
17    3 -1.22E-3 -17 (-14:15:16)      $ air around the pipe
18    4 -0.936   -18 17              $ Borated Polyethylene
19    4 -0.936   -19 18              $ Borated Polyethylene
20    4 -0.936   -20 19              $ Borated Polyethylene
21    4 -0.936   -21 20              $ Borated Polyethylene
22    4 -0.936   -22 21              $ Borated Polyethylene
23    4 -0.936   -23 22              $ Borated Polyethylene
24    4 -0.936   -24 23              $ Borated Polyethylene
25    4 -0.936   -25 24              $ Borated Polyethylene
26    4 -0.936   -26 25              $ Borated Polyethylene
27    4 -0.936   -27 26              $ Borated Polyethylene
28    5 -7.86    -28 27              $ SS Plate
29    5 -7.86    -29 28              $ SS Plate
```

```
30    5 -7.86    -30 29              $ SS Plate
31    5 -7.86    -31 30              $ SS Plate
32    5 -7.86    -32 31              $ SS Plate
47    3 -1.22E-3 -90  32               $ Outside World
90    0          90                 $ Void

c ===========================================================================
c SURFACE CARD
c ===========================================================================
10  1  rpp -0.25 0.25 -1 1 -4.5 4.5              $ Al block
11  1  rpp 0.25 0.253 -1 1 -4.5 4.5              $ Bismuth-209
12    cz  8.25                            $ Al back plate cylinder
13    pz -6                               $ Backing Plate Plane (Top)
14    pz -7.2                             $ Backing Plate Plane (Bottom)
15    cz 8.55                             $ Beam Line Pipe Cylinder
16    pz 10                               $ Beam Line Pipe plane
17    rpp -15.00 15.00 -15.00 15.00 -24.92 20.00   $ 2" of Borated Polyethylene
18    rpp -15.51 15.51 -15.51 15.51 -25.43 20.51   $ 2" of Borated Polyethylene
19    rpp -16.02 16.02 -16.02 16.02 -25.94 21.02   $ 2" of Borated Polyethylene
20    rpp -16.52 16.52 -16.52 16.52 -26.44 21.52   $ 2" of Borated Polyethylene
21    rpp -17.03 17.03 -17.03 17.03 -26.95 22.03   $ 2" of Borated Polyethylene
22    rpp -17.54 17.54 -17.54 17.54 -27.46 22.54   $ 2" of Borated Polyethylene
23    rpp -18.05 18.05 -18.05 18.05 -27.97 23.05   $ 2" of Borated Polyethylene
24    rpp -18.56 18.56 -18.56 18.56 -28.48 23.56   $ 2" of Borated Polyethylene
25    rpp -19.06 19.06 -19.06 19.06 -28.98 24.06   $ 2" of Borated Polyethylene
26    rpp -19.57 19.57 -19.57 19.57 -29.49 24.57   $ 2" of Borated Polyethylene
27    rpp -20.08 20.08 -20.08 20.08 -30.00 25.08   $ 2" of Borated Polyethylene
28    rpp -20.33 20.33 -20.33 20.33 -30.25 25.33   $ 0.5" of SS Plate
29    rpp -20.59 20.59 -20.33 20.33 -30.51 25.59   $ 0.5" of SS Plate
30    rpp -20.84 20.84 -20.59 20.59 -30.76 25.84   $ 0.5" of SS Plate
31    rpp -21.10 21.10 -20.59 20.59 -31.02 26.10   $ 0.5" of SS Plate
```

```
32     rpp -21.35 21.35 -20.59 20.59 -31.27 26.35   $ 0.5" of SS Plate
90     so 300                          $ Tally ROI & Outside Environment

c ===========================================================================
c DATA CARD
c ===========================================================================
c Target Plate offset by 10 Degrees
*TR1 0 0 0 10 90 80 90 0 90 100 90 10
c
c Polyethylene Block Translocation
TR2 0 0 -30 1 0 0 0 1 0 0 0 1
TR3 -22.62 0 0 1 0 0 0 1 0 0 0 1
TR4 22.62 0 0 1 0 0 0 1 0 0 0 1
c
MODE N H D T P A S #
IMP:N 1 21R 0
IMP:P 1 21R 0
IMP:H 1 21R 0
IMP:D 1 21R 0
IMP:A 1 21R 0
IMP:T 1 21R 0
IMP:S 1 21R 0
IMP:# 1 21R 0
c
PHYS:N 100 0 0 -1 -1 0 2
PHYS:H 100 0 -1 J 0 J 1
PHYS:A 100 3j 0
PHYS:# 140 J J J 0
c
CUT:# J 0.01
CUT:H J 0.01
```

```
CUT:A J 0.01
CUT:D J 0.01
CUT:S J 0.01
CUT:N J 1e-9
c
LCA 2 1 1 23 1 1 0 1 0
c
sdef PAR=1 x=d1 y=d2 z=d3 CCC=11 ERG=d4 VEC=0 0 -1 DIR=d5 EFF=0.0001
SI1  -0.4 0.9
SP1  0 1
SI2 -1 1
SP2  0 1
SI3 -3.5 3.5
SP3  0 1
SI4 H 0 0.001 0.002 0.005 0.01 0.05 0.1 0.5 1 1.5 2 2.5 3 3.5 4 4.5 5 5.5 6 6.5
    7 7.5 8 8.5 9 9.5 10 10.5 11 11.5 12 12.5
SP4 D 0 0.001406153 0.002831182 0.007373327 0.014942203 0.066366757 0.112268423
    0.212833861 0.194489262 0.148338576 0.102227302 0.06804882 0.032269259
    0.018947065 0.008382303 0.004312252 0.002205652 0.001131632 0.000618138
    0.000351801 0.000223496 0.000145165 0.00010153 6.85231E-05 4.80271E-05
    3.03043E-05 1.97037E-05 1.02224E-05 5.99723E-06 1.82244E-06 1.22686E-06
    1.27672E-08
SI5  -1 9i 1
SP5   0 0.10 9r
SB5   0 0.02 8r 0.84
c ----
PTRAC cell=17 max=10000 TYPE=N FILE=asc
c ----
c Rectangular mesh
tmesh
rmesh1:N
```

```
cora1 -27 53i 27
corb1 -27 53i 27
corc1 -54 29i -24
rmesh11:P
cora11 -27 53i 27
corb11 -27 53i 27
corc11 -54 29i -24
endmd
c ===========================================================================
c Neutron,  Photon Tally 1 m from Origin Ring Detector
c ===========================================================================
F15z:n 0 100 0.0
E15   0 1E-7 1E-3 0.5 1 14i 15
c
F25z:p 0 100 0.0
E25   0.001 0.5 1 14i 15
c ===========================================================================
c Neutron,  Photon Point Detector Tally @ 1 M from source w/ shielding
c ===========================================================================
F35:n 0 0 -100 0.0
de35  log 2.5E-8  1.0E-7  1.0E-6  1.0E-5 1.0E-4 1.0E-3 1.0E-2 1.0E-1 5.0E-1
       1.0     2.0     5.0    10.0   20.0
C MESH OF FLUX TO DOSE CONVERSION FACTOR VALUES ICRP-21 (REM/h per unit flux)
df35  log 3.85E-6 4.17E-6 4.55E-6 4.35E-6 4.17E-6 3.70E-6 3.57E-6 2.08E-5
       7.14E-5 1.18E-4 1.43E-4 1.47E-4 1.473E-4 1.54E-4
c
F45:p 0 0 -100 0.0
de45  log 0.01    0.015   0.02    0.03    0.04    0.05    0.06
       0.08    0.1     0.15    0.2     0.3     0.4     0.5
       0.6     0.8     1.0     1.5     2.0     3.0     4.0
       5.0     6.0     8.0     10.0
```

```
C MESH OF FLUX TO DOSE CONVERSION FACTOR VALUES ICRP-21 (REM/h per unit flux)
df45  log 2.78e-6 1.11e-6 5.88e-7 2.56e-7 1.56e-7 1.20e-7 1.11e-7
        1.20e-7 1.47e-7 2.38e-7 3.45e-7 5.56e-7 7.69e-7 9.09e-7
        1.14e-6 1.47e-6 1.79e-6 2.44e-6 3.03e-6 4.00e-6 4.76e-6
        5.56e-6 6.25e-6 7.69e-6 9.09e-6
c
F55:n 0 0 -100 0.0
E55   0 1E-7 1E-3 0.5 1 14i 15
c
F65:p 0 0 -100 0.0
E65   0.001 0.5 1 14i 10
c
c End Tally
m1     13027 -1.00
m2     83209 -1.00
c air internet 15 deg at sea level
m3 7014.66c -0.745962 8016.66c -0.228590 18000.42c -2.5448e-2 GAS=1
c 5% Borated Polyethylene
c Source:  TART LLNL
c Specified elemental Composition
c Total Mass Density :     0.936 g/cm^3
c
m4    1001 -0.11598
      1002 -0.00002
      5010 -0.0098
      5011 -0.0402
      6000 -0.612
      8016 -0.222
mt4 poly.10t
c
c SS Plate for Gammas
```

```
m5    26000 -0.9865
       6000 -0.0015
      25055 -0.0060
      14000 -0.0060
c ------------------------------------------------
NPS 1000000
c PRDMP 1E5 1E5
```

VITA

Name: Viharkumar Satish Bhakta

Address: 129 Zachry Engineering Center
3133 TAMU
College Station, TX 77843-3133

Email Address: bhaktavs@gmail.com

Education: M.S., Health Physics, Texas A&M University, 2011
B.S., Nuclear Engineering, Texas A&M University, 2009